Effectiveness of smearing methods studied with Monte Carlo renormalization group tools

Faruk Geles

Diplomarbeit

zur Erlangung des akademischen Grades eines
Magisters
an der Naturwissenschaftlichen Fakultät der
Karl-Franzens-Universität Graz

Betreuer: Univ.-Prof. Dr. phil. Christian B. Lang
Institut für Physik, Fachbereich Theoretische Physik

2011

Contents

1 INTRODUCTION

In the standard model of elementary particle physics several interactions are included. One of them is Quantum Chromodynamics(QCD), the theory of strong interaction. Because of the strength of this interaction the perturbation theory can not be applied to the whole theory. Only in some regimes it is tolerable. Since the definition of QCD few non-perturbative approaches have been devised. The most promising of these methods is the definition of QCD on a 4 dimensional lattice, which was first introduced by Wilson [1]. For QCD on the lattice many tools have been introduced to obtain better results. One class of these methods are referred to as smearing methods. They are widely used in the treatment of Quantum Chromodynamics on the lattice. There are many types of smearing methods. Some of them are APE-smearing, HYP smearing, p-APE smearing, p-HYP smearing, n-APE smearing, n-HYP smearing, STOUT smearing, logarithmic link smearing, AUS smearing etc.

One of the aims of the smearing methods is to reduce the effect of the fluctuations of the gauge fields in order to improve the accessibility of the signals. Smearing methods are also part of the algorithm for the generation of the gauge configurations to reach better acceptance rates. Another use of the smearing methods is to enhance the flavor symmetry, which appears in staggered lattice QCD because of the distribution of the Dirac spinor components to different lattice sites. They also reduce discretization errors and suppress exceptional configurations. All of these reasons contribute to extraction of better information from QCD. Therefore these reasons make the smearing methods an interesting area.

The aim of this diploma thesis is to test the effectiveness of the most used smearing methods. This could simplify the classification of the smearing methods and could also help to construct better smearing methods with less effort. Here a powerful tool, referred to as the Monte Carlo renormalization group (a combination of the Monte Carlo methods and renormalization group), is used.

We proceed step by step and make many preparations for our investigation. The composition of this work is the following. In Chapter 2 and 3 some basics of lattice QCD are refreshed. They start from the construction of the QCD Lagrangian and extracting its symmetries. Then path integral methods are used to discretize the system and to translate it to the lattice. Through this approach, Monte Carlo methods can be used to extract information from the QCD defined on the lattice. In Chapter 3 we therefore start with a Monte Carlo simulation of a pure gauge theory. The inclusion of the quark fields brings us to the so called Hybrid Monte Carlo algorithm, which is a combination of Monte Carlo methods and Molecular Dynamics. We use the configurations which are generated with this algorithm for two mass degenerate quarks and give the general ideas how such an algorithm is implemented.

We then describe some of the most common smearing methods in Chapter 4. This chapter includes testing the effect of the smearing methods on the static quark potential.

In Chapter 5 we give the definition of some local observables on the lattice and finally use these observables, and the smearing methods from Chapter 4 and additionally use some Monte Carlo renormalization group tools, to examine the effectiveness of our smearing methods in the last chapter.

2 LATTICE GAUGE THEORY

2.1 Introduction

Gauge theories are believed to underlie all elementary particle interactions. A systematic approach is with a Lagrangian formulation of the field theory. In field theory one is dealing with fields. Field variables are functions of space and time: $\Phi_i(x, y, z, t)$. The Lagrangian (or Lagrangian density) is a function of Φ_i and their space-time derivatives. In a relativistic field theory space and time coordinates are treated on equal footing. Using this feature the generalized Euler Lagrange equations can be written as

$$\partial_\mu \left(\frac{\partial \mathcal{L}}{\partial(\partial_\mu \Phi_i)} \right) = \frac{\partial \mathcal{L}}{\partial \Phi_i}. \tag{2.1}$$

Our first aim is to find the Lagrangian and its symmetries for the strong interaction. Therefore we start with an simpler theory and generalize this to the much more complicated theory of the strong interaction. Then we will go on to the discretization of this theory on the lattice.

2.2 Abelian and non-Abelian Gauge Theories

2.2.1 Quantum Electrodynamics

Before we write down the quantum electrodynamics (QED) Lagrangian let us look at the Dirac Lagrangian for a spinor (spin 1/2) field. We assume that we have a spinor field ψ and the Lagrangian is given by

$$\mathcal{L} = i\overline{\psi}\gamma^\mu \partial_\mu \psi - m\overline{\psi}\psi, \tag{2.2}$$

where ψ and $\bar{\psi}$ are independent field variables. Applying the Euler Lagrange equation to $\overline{\psi}$ one gets

$$(i\gamma^\mu \partial_\mu - m)\psi = 0. \tag{2.3}$$

This is the Dirac equation, which describes a fermion with mass m. The second Lagrangian we want to discuss is the Maxwell Lagrangian for a massless vector field with a source term

$$\begin{aligned} \mathcal{L} &= -\frac{1}{4} F^{\mu\nu} F_{\mu\nu} - e J^\mu A_\mu \\ &= -\frac{1}{4} F^{\mu\nu} F_{\mu\nu} - e\overline{\psi}\gamma^\mu \psi A_\mu, \end{aligned} \tag{2.4}$$

where A_μ is the electromagnetic vector potential and $F^{\mu\nu}$ is the electromagnetic field tensor which is defined by

$$F^{\mu\nu} = \partial^\mu A^\nu - \partial^\nu A^\mu. \tag{2.5}$$

In the same way applying the Euler Lagrange equation yields the Maxwell equations

$$\partial_\mu F^{\mu\nu} = eJ^\nu. \tag{2.6}$$

We can combine these two Lagrangians to write down the Lagrangian for Quantum Electrodynamics (QED)

$$\mathcal{L} = \overline{\psi}(i\gamma^\mu\partial_\mu - m)\psi - \frac{1}{4}F^{\mu\nu}F_{\mu\nu} - e\overline{\psi}\gamma^\mu\psi A_\mu. \tag{2.7}$$

Now we want to identify the symmetries of this Lagrangian, i.e., the transformations, which leave this Lagrangian invariant. Therefore it is appropriate to start again with Dirac Lagrangian for a spin 1/2 field (2.2). Obviously a global phase transformation or gauge transformation of the form

$$\psi \to e^{i\alpha}\psi \tag{2.8}$$

leaves this Lagrangian invariant [2]. The next step is to test the local gauge transformation behavior of this Lagrangian. A local gauge transformation is defined by

$$\psi \to e^{i\alpha(x)}\psi. \tag{2.9}$$

In this case a local gauge transformation is a phase rotation $\alpha(x)$ which varies from point to point. The straightforward attempt to check the local gauge invariance of this Lagrangian under such a transformation would fail. However it is possible to rewrite this Lagrangian in such a way that it is invariant under such transformations as well. For the mass term part there are no restrictions in connection with global and local phase transformations. Complications arise by including derivatives. The derivative of the field $\psi(x)$ in direction n^μ is defined by

$$n^\mu\partial_\mu\psi = \lim_{\epsilon\to 0}\frac{\psi(x+n\epsilon)-\psi(x)}{\epsilon}. \tag{2.10}$$

Here we are subtracting two different fields with different phase transformations. In some sense to compensate the difference in phase transformations we can define a quantity $U(x,y)$ called comparator (or gauge transporter) which depends on the two points and has the following transformation law

$$U(x,y) = e^{i\alpha(x)}U(x,y)e^{-i\alpha(y)}, \tag{2.11}$$

with

$$U(y,y) = 1. \tag{2.12}$$

We can consider $U(x,y)$ as a pure phase. The objects $\psi(y)$ and $U(y,x)\psi(x)$ have the same transformation law. This fact can be used to define the so called covariant derivative

$$n^\mu \mathcal{D}_\mu \psi = \lim_{\epsilon\to 0} \frac{\psi(x+\epsilon n) - U(x+\epsilon n, x)\psi(x)}{\epsilon}. \tag{2.13}$$

If we assume that the comparator $U(x,y)$ is a continuous function of the positions x and y, then it can be expanded in the separation of two points

$$U(x+\epsilon n, x) = 1 - ie\epsilon n^\mu A_\mu(x) + O(\epsilon^2). \tag{2.14}$$

Here the coefficient of the displacement ϵn^μ is a new vector field $A_\mu(x)$ and e is an arbitrary extracted constant. This field appears as the infinitesimal limit of a comparator of local symmetry transformations. It is called connection. If we insert (2.14) in (2.13) the covariant derivative takes the form

$$\mathcal{D}_\mu\psi(x) = \partial_\mu\psi(x) + ieA_\mu\psi(x) = (\partial_\mu + ieA_\mu)\psi(x). \tag{2.15}$$

One can use the relations above to find the transformation law for the $A_\mu(x)$ under local gauge transformation. This is done by inserting (2.14) in (2.11). The result is

$$A_\mu(x) \to A_\mu(x) - \frac{1}{e}\partial_\mu\alpha(x). \tag{2.16}$$

Now we want to test if the covariant derivative $\mathcal{D}$ transforms in same way as the field $\psi(x)$:

$$\begin{aligned}
\mathcal{D}_\mu\psi(x) &\to [\partial_\mu + ie(A_\mu(x) - \frac{1}{e}\partial_\mu\alpha(x))]e^{i\alpha(x)}\psi(x) \\
&= i(\partial_\mu\alpha(x))e^{i\alpha(x)}\psi(x) + e^{i\alpha(x)}\partial_\mu\psi(x) \\
&+ ieA_\mu(x)e^{i\alpha(x)}\psi(x) - i(\partial_\mu\alpha(x))e^{i\alpha(x)}\psi(x) \\
&= e^{i\alpha(x)}(\partial_\mu + ieA_\mu)\psi(x) \\
&= e^{i\alpha(x)}\mathcal{D}_\mu\psi(x).
\end{aligned} \tag{2.17}$$

In fact our result shows that the covariant derivative $\mathcal{D}_\mu$ transforms in the same way as the field ψ. At this stage we have derived the covariant derivative and the transformation law for the vector field from the local phase rotation symmetry. To write down the whole Lagrangian we also need the kinetic term for the field $A_\mu(x)$. We have seen that the covariant derivative has the same transformation law as the field ψ. The commutator of covariant derivatives has the same transformation law

$$[\mathcal{D}_\mu, \mathcal{D}_\nu]\psi(x) \to e^{i\alpha(x)}[\mathcal{D}_\mu, \mathcal{D}_\nu]\psi(x). \tag{2.18}$$

This is because calculating the commutator gives

$$\begin{aligned}
[\mathcal{D}_\mu, \mathcal{D}_\nu] &= [\partial_\mu + ieA_\mu(x), \partial_\nu + ieA_\nu(x)] \\
&= [\partial_\mu, \partial_\nu] + ie([\partial_\mu, A_\nu] - [\partial_\nu, A_\mu]) - e^2[A_\mu, A_\nu] \\
&= ie(\partial_\mu A_\nu - \partial_\nu A_\mu) \\
&= ieF_{\mu\nu},
\end{aligned} \tag{2.19}$$

which is gauge invariant

$$\begin{aligned}
[\mathcal{D}_\mu, \mathcal{D}_\nu] &\rightarrow [\mathcal{D}'_\mu, \mathcal{D}'_\nu] \\
&= ie(\partial_\mu A'_\nu - \partial_\nu A'_\mu) \\
&= ie(\partial_\mu [A_\nu(x) - \frac{1}{e}\partial_\nu \alpha(x)] - \partial_\nu [A_\mu(x) - \frac{1}{e}\partial_\mu \alpha(x)]) \\
&= ieF_{\mu\nu}. \qquad (2.20)
\end{aligned}$$

After we have seen the invariance of $F_{\mu\nu}$, one can now write the whole local gauge invariant Lagrangian for the electron field and its associated connection A_μ

$$\mathcal{L} = \overline{\psi}(i\gamma^\mu \mathcal{D}_\mu - m)\psi - \frac{1}{4}F^{\mu\nu}F_{\mu\nu}. \qquad (2.21)$$

The substitution of $\mathcal{D}_\mu$ for ∂_μ converts a global invariant Lagrangian into a local invariant Lagrangian. The covariant derivative introduces a new vector field. This fields are called gauge fields [3]. The idea of gauge invariance was introduced by Hermann Weyl [4]. A global phase transformation can be thought as a multiplication of ψ by a complex phase U:

$$\psi \rightarrow U\psi \quad \text{where} \quad U^\dagger U = 1 \qquad (2.22)$$

with the definition $U = e^{i\theta}$. The group of all such phases is U(1). The symmetry involved is called U(1) gauge invariance. The fact that QED is invariant under a large group of transformations allows an independent symmetry transformation at every point in space-time. The gauge symmetry is a fundamental principle which determines the form of the QED Lagrangian. The gauge symmetry group for QED is U(1). In year 1954 Yang and Mills have applied the same idea to the group SU(2) [5]. Later it was extended to color SU(3) leading to Chromodynamics. In the Standard Model all fundamental interactions are generated in this way.

2.2.2 Quantum Chromodynamics

After studying the symmetry group of the QED (phase rotation invariance for Quantum Electrodynamics) we want now to generalize this treatment to Quantum Chromodynamics. Quantum Chromodynamics is the theory of strong interacting particles and fields. This theory has two fields: the quarks and gluons. The quarks are spin 1/2 particles and interact strongly via gluons, the intermediate particles. The gluons are spin 1 particles and obey Bose statistics. The quarks come in six different flavors called up, down, charm, strange, top, bottom and they are building mesons and hadrons. The force between these quarks is mediated through gluons.

The naive quark model seems to violate Pauli's exclusion principle because for example the particle Δ^{++} is supposed to consist of 3 identical u quarks. O. W. Greenberg, M. Gell-Mann, H. Fritzsch and H. Leutwyler have suggested that the quarks come not only in six flavors but also in three colors [6, 7]. Although the quarks with different flavors

carry different masses, the three colors (for a given flavor) correspond to the same mass parameter. The Lagrangian for a free flavor can be written as

$$\begin{aligned}\mathcal{L} &= [i\overline{\psi_r}\gamma^\mu\partial_\mu\psi_r - m\overline{\psi_r}\psi_r] + [i\overline{\psi_b}\gamma^\mu\partial_\mu\psi_b - m\overline{\psi_b}\psi_b] \\ &+ [i\overline{\psi_g}\gamma^\mu\partial_\mu\psi_g - m\overline{\psi_g}\psi_g].\end{aligned} \tag{2.23}$$

We next introduce the compact notation

$$\psi = \begin{pmatrix}\psi_r \\ \psi_b \\ \psi_g\end{pmatrix},$$

$$\overline{\psi} = \begin{pmatrix}\overline{\psi_r} & \overline{\psi_b} & \overline{\psi_g}\end{pmatrix}. \tag{2.24}$$

With this notation we can write our Lagrangian as

$$\mathcal{L} = i\overline{\psi}\gamma^\mu\partial_\mu\psi - m\overline{\psi}\psi. \tag{2.25}$$

The procedure is again the same as in QED. One is interested in the symmetries of this Lagrangian. Therefore we investigate the behavior of the Lagrangian under a global gauge transformation

$$\psi \to U\psi, \qquad (\overline{\psi} \to \overline{\psi}U^\dagger), \tag{2.26}$$

where U is a unitary 3×3 Matrix. Any unitary matrix can be written as the exponential function of a Hermitian matrix H:

$$U = e^{iH}. \tag{2.27}$$

Such a Hermitian matrix can be constructed as

$$H = \alpha\mathbb{1} + \frac{\lambda^k}{2}a^k, \tag{2.28}$$

where (for U(3) algebra) α, $a^1, a^2, ...a^8$ are 9 real numbers, $\lambda^1, \lambda^2, ...\lambda^8$ are the so called Gell-Mann matrices and we use the "sum convention". Hence:

$$U = e^{i(\alpha\mathbb{1}+\frac{\lambda^k}{2}a^k)} = e^{i\alpha}e^{i\frac{\lambda^k}{2}a^k}. \tag{2.29}$$

The first term is only a phase transformation like in case of U(1) and the second term $e^{i\frac{\lambda^k}{2}a^k}$ is a matrix with determinant 1 and belongs to the group SU(3) [2]. This global transformation can be made local by defining the space-time dependence of a

$$\psi \to e^{i\frac{\lambda^k}{2}a^k(x)}\psi = e^{it^k a^k(x)}\psi. \tag{2.30}$$

Here we replace

$$\frac{\lambda^k}{2} \to t^k \tag{2.31}$$

for simplicity. In the implementation of local gauge invariance of the Lagrangian additional complications arise, because of the non-Abelian symmetry group of more general theories. The field theory with a non-commuting local symmetry is called non-Abelian gauge theory. The procedure of constructing a local gauge invariant Lagrangian is again the same like in the case of QED. There are again problems with the derivative in the Lagrangian. It has to be replaced by a more generalized derivative the so-called covariant derivative. We can construct the derivative with the help of the so-called comparator U, which in this case is a 3×3 matrix. The transformation law for the comparator in this case is given by

$$\begin{aligned} U(x,y) &\to \Omega(x)U(x,y)\Omega^\dagger(y) \\ &= e^{i\alpha^k(x)t^k}U(x,y)e^{-i\alpha^k(y)t^{k\dagger}}. \end{aligned} \tag{2.32}$$

Again we set $U(y,y) = 1$. Near $U = 1$ such a matrix can be expanded in terms of Hermitian generators of SU(3) for an infinite decimal separation

$$U(x+\epsilon n, x) = 1 + ig\epsilon n^\mu A_\mu^k t^k + O(\epsilon^2). \tag{2.33}$$

The next step is to put this expression into the definition of the covariant derivative from the last section, which was defined as

$$n^\mu \mathcal{D}_\mu \psi = \lim_{\epsilon\to 0} \frac{\psi(x+\epsilon n) - U(x+\epsilon n, x)\psi(x)}{\epsilon}.$$

Finally the covariant derivative becomes

$$\mathcal{D}_\mu = \partial_\mu - igA_\mu^k t^k. \tag{2.34}$$

One can now derive the transformation law for the connection A_μ^k in a similar way as in QED. The result is

$$A_\mu^k t^k \to \Omega(x)\left(A_\mu^k t^k + \frac{i}{g}\partial_\mu\right)\Omega^\dagger(x). \tag{2.35}$$

At this stage we are ready to look at the transformation behavior of the covariant

derivative:

$$\begin{aligned}
\mathcal{D}_\mu\psi &= (\partial_\mu - igA^k_\mu t^k)\psi \\
&\to \left[\partial_\mu - ig\left(\Omega(x)\left(A^k_\mu t^k + \frac{i}{g}\partial_\mu\right)\Omega^\dagger(x)\right)\right]\Omega(x)\psi \\
&= \left[\partial_\mu - ig\left((1+i\alpha^k t^k)\left(A^i_\mu t^k + \frac{i}{g}\partial_\mu\right)(1-i\alpha^j t^j)\right)\right](1+i\alpha^l t^l)\psi \\
&= \left[\partial_\mu - igA^k_\mu t^k - i(\partial_\mu\alpha^k)t^k + g[\alpha^k t^k, A^j_\mu t^j]\right](1+i\alpha^l t^l)\psi \\
&= (1+i\alpha^k t^k)\mathcal{D}_\mu\psi. \qquad (2.36)
\end{aligned}$$

In this verification we include $\Omega(x) = e^{i\alpha^k(x)t^k}$ only up to the first order expansion in $\alpha(x)$ because the exponent does not commute with the derivative. This result shows that the covariant derivative has the same transformation law as the field ψ. After this we are now prepared to write down the local gauge invariant Lagrangian with the interaction term

$$\mathcal{L} = \overline{\psi}(i\gamma^\mu\mathcal{D}_\mu - m)\psi - \frac{1}{4}(F^k_{\mu\nu})^2. \qquad (2.37)$$

The open point is to show the local gauge invariance of the field tensor $F^k_{\mu\nu}$. This can be shown if one calculates the commutator relation of two covariant derivatives

$$\begin{aligned}
[\mathcal{D}_\mu, \mathcal{D}_\nu] &= \left[\partial_\mu - igA^k_\mu t^k, \partial_\nu - igA^j_\nu t^j\right] \\
&= -ig(\partial_\mu A^k_\nu t^k - \partial_\nu A^k_\mu t^k - ig[A^k_\mu t^k, A^j_\nu t^j]) \\
&= -ig(\partial_\mu A^k_\nu - \partial_\nu A^k_\mu + gf^{kjl}A^j_\mu A^l_\nu)t^k \\
&= -igF^k_{\mu\nu}t^k, \qquad (2.38)
\end{aligned}$$

where we have used the commutation relation for Gell-Mann matrices

$$[t^i, t^j] = if^{ijk}t^k, \qquad (2.39)$$

where f^{ijk} is a set of the numbers called the structure constants. It is equivalent to ϵ_{ijk} for SU(2). So the field strength tensor for Quantum Chromodynamics becomes

$$F^i_{\mu\nu} = \partial_\mu A^i_\nu - \partial_\nu A^i_\mu - gf^{ijk}A^j_\mu A^k_\nu.$$

This calculation shows that the field strength tensor is no longer a gauge invariant quantity, because for the last term the commutation relation does not vanishes any more. There are now 8 field strength tensors and each is associated with a given rotation in an abstract space. One can take a gauge invariant combination of field strengths

$$\mathcal{L} = -\frac{1}{2}\mathrm{tr}\left[\left(F^k_{\mu\nu}t^k\right)^2\right] = -\frac{1}{4}(F^k_{\mu\nu})^2. \qquad (2.40)$$

This is exactly the kinetic part of the Lagrangian. From the definition of the field strength tensor it is obvious that the kinetic part of the Lagrangian contains terms which are cubic and quartic in A^i_μ. Consequently the interaction differs from the interaction in QED [3]. The nature of QCD is quite different. This gauge symmetry group is the SU(3). After some study of the symmetry group of QCD, in the next step we want to look the quantization of such a theory.

2.3 Quantization of a Gauge theory

2.3.1 Path Integral

Path integrals or functional integrals provide an easy road to the quantization. In classical mechanics a path in space-time plane describes the motion of a particle. In quantum mechanics all paths are important in the description of the motion of a particle and the propagator is given by

$$\begin{aligned} K &= \int dx_1 ... dx_N \exp\left(iS[x(t), \dot{x}(t)]\right) \\ &= \int \mathcal{D}x(t) \exp\left(iS[x(t), \dot{x}(t)]\right). \end{aligned} \tag{2.41}$$

This relation for the propagator says that a particle which moves from one position to another takes virtually all possible paths between these two positions. The analogon of the quantum mechanical propagator in quantum field theory is given by

$$\begin{aligned} K &= \int d\psi_1 ... d\psi_N \exp\left(iS[\psi]\right) \\ &= \int \mathcal{D}\psi \exp\left(iS[\psi]\right), \end{aligned} \tag{2.42}$$

where S is the field action defined by

$$S = \int d^4x \mathcal{L}(\psi, \partial_\mu \psi). \tag{2.43}$$

The idea of path integrals can be translated to statistical mechanics as well. A path integral can be written as a partition function

$$Z = \sum_j \exp(\beta E_j), \tag{2.44}$$

(where j denotes spin configurations) which is the central object in statistical mechanics. The "translation" can be done via a Wick rotation, when we switch from from real time τ to imaginary time $t = i\tau$ and rotate the contour integration, the action becomes

$$S = iS_E. \tag{2.45}$$

So our propagator can be written as a partition function

$$Z = \int \mathcal{D}\psi \exp\left(-S_E[\psi]\right). \tag{2.46}$$

defined by associating to each path a statistical weight e^{-S_E} where S_E is the Euclidean action obtained from the usual Minkowski action by Wick rotation. Notice here we have changed the letter K through Z, because the Wick rotation translates our propagator to a partition function. Let us go a step further and look at the expectation value of a time ordered product of Heisenberg field operators (which is known as Green's function or as correlation function):

$$\left\langle 0 \left| T\hat{\phi}(x_1)\hat{\phi}(x_2).....\hat{\phi}(x_n) \right| 0 \right\rangle. \tag{2.47}$$

The order of these operators are such that the "earlier" field is written to the right of the "later". The Green's functions are related to the amplitudes of physical processes such as scattering or decay processes. Let us calculate the two point function via path integral. This results in

$$\left\langle 0 \left| T\hat{\phi}(x_1)\hat{\phi}(x_2) \right| 0 \right\rangle = \frac{\int \mathcal{D}\phi \ \hat{\phi}(t_1)\hat{\phi}(t_2) \exp\left(iS[\psi]\right)}{\int \mathcal{D}\psi \ \exp\left(iS[\psi]\right)}. \tag{2.48}$$

The expectation value of a field can be calculated according to

$$\left\langle 0 \left| \hat{\phi}(x_1) \right| 0 \right\rangle = \frac{\int \mathcal{D}\phi \ \hat{\phi}(t_1) \exp\left(iS[\psi]\right)}{\int \mathcal{D}\psi \ \exp\left(iS[\psi]\right)}. \tag{2.49}$$

The idea of the Wick rotation can again be applied [8]:

$$\left\langle 0 \left| T\hat{\phi}(x_1)\hat{\phi}(x_2) \right| 0 \right\rangle = \frac{\int \mathcal{D}\phi \ \hat{\phi}(t_1)\hat{\phi}(t_2) \exp\left(-S_E[\psi]\right)}{\int \mathcal{D}\psi \ \exp\left(-S_E[\psi]\right)}, \tag{2.50}$$

$$\left\langle 0 \left| \hat{\phi}(x_1) \right| 0 \right\rangle = \frac{\int \mathcal{D}\phi \ \hat{\phi}(t_1) \exp\left(-S_E[\psi]\right)}{\int \mathcal{D}\psi \ \exp\left(-S_E[\psi]\right)}. \tag{2.51}$$

2.3.2 Path Integral for QCD

Now we are going to apply these ideas to QCD, and formulate it on the Euclidean lattice. First we want to study the QCD action functional on the lattice. This will help us for the discretization of QCD on the lattice. We start with the QCD action. Then we will discuss the discretization of lattice action for fermions and gluons. At the end we will write down a complete expression for the QCD lattice path integral. We start with the definition of a 4-dimensional hypercubic lattice

$$\Lambda \ = \ \{n = (n_1, n_2, n_3, n_4)\}, \tag{2.52}$$

where

$$n_1, n_2, n_3 \quad = \quad 0, 1, ..., N-1; n_4 = 0, 1, ..., N_T - 1. \tag{2.53}$$

The fermionic part of the Euclidean QCD action for one flavor is given by

$$S_F^0[\psi, \overline{\psi}] \quad = \quad \int d^4x \; \overline{\psi}(\gamma_\mu \partial_\mu + m)\psi. \tag{2.54}$$

We can write down the lattice version of this free fermion action as

$$S_F^0[\psi, \overline{\psi}, A] \quad = \quad a^4 \sum_{n \in \Lambda} \overline{\psi}(n) \left(\sum_{\mu=1}^{4} \gamma_\mu \frac{\psi(n+\hat{\mu}) - \psi(n-\mu)}{2a} + m\psi(n) \right). \tag{2.55}$$

One can again, like in the continuum case, study the behavior of the lattice action under gauge transformations like $\Omega(n)$ of SU(3) for each lattice site n

$$\psi(n) \to \psi'(n) = \Omega(n)\psi \qquad \overline{\psi}(n) \to \overline{\psi}'(n) = \overline{\psi}(n)\Omega(n)^\dagger. \tag{2.56}$$

The idea for implementation of gauge invariance is the same like the comparator which we have introduced earlier. In lattice gauge theory one introduces a field U_μ, which lives between the spinor fields $\psi(n)$ on the lattices sites. The task of this field is to restore the gauge invariance. This restriction implies the gauge transformation of the field U_μ as

$$U_\mu(n) \quad \to \quad U'_\mu(n) = \Omega(n) U_\mu(n) \Omega(n+\hat{\mu})^\dagger \tag{2.57}$$

These introduced gauge fields U_μ are elements of the SU(3) gauge group. They are often referred to as link variables U_μ which live on the links connecting the neighboring sites. From these arguments we see that the link variables are oriented i.e.

$$U_{-\mu}(n) = U_\mu(n-\hat{\mu})^\dagger. \tag{2.58}$$

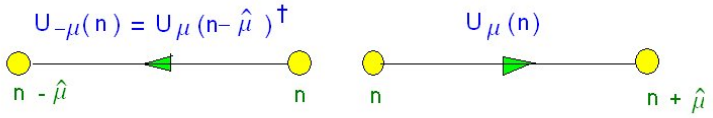

Figure 2.1: Orientation of the link variables.

Link variables with their properties can be used to rewrite the free fermion action in an external gauge field U_μ

$$S_F[\psi, \overline{\psi}, U] \quad = \quad a^4 \sum_{n \in \Lambda} \overline{\psi}(n) \left(\sum_{\mu=1}^{4} \gamma_\mu \frac{U_\mu(n)\psi(n+\hat{\mu}) - U_{-\mu}(n)\psi(n-\mu)}{2a} + m\psi(n) \right) \tag{2.59}$$

which is gauge invariant. The link variables are the lattice version of the continuum gauge transporters which are defined as

$$U(x,y) = P \exp\left(i \int_{C_{xy}} A \cdot ds \right). \tag{2.60}$$

This definition says that a gauge transporter is a path ordered exponential of the gauge field A_μ along some curve C_{xy} connecting two point x and y. Additionally it has the same gauge transformation. So we can use this equivalence to write our link variables explicitly as

$$U_\mu(n) = \exp\left(iaA_\mu(n)\right), \tag{2.61}$$

where $A_\mu(n)$ are algebra valued gauge fields. To check the gauge invariance of our new action, we can expand (2.61) for small a

$$U_\mu(n) = \mathbb{1} + iaA_\mu(n) + \mathcal{O}(a^2) \qquad U_{-\mu}(n) = \mathbb{1} - iaA_\mu^\dagger(n-\hat{\mu}) + \mathcal{O}(a^2) \tag{2.62}$$

and insert these expressions in (2.59) and for $a \to 0$ we find the continuum gauge invariant action

$$S_F[\psi, \overline{\psi}, A] = \int d^4x \overline{\psi}(\gamma_\mu \left(\partial_\mu + iA_\mu\right) + m)\psi. \tag{2.63}$$

After we have devised the lattice fermionic part of the action, the next step is the construction of the lattice gauge part of the action. Let us look at a gauge invariant product of the link variables along a closed loop $\mathcal{P}$

$$L[U] = \mathrm{tr}\left[\prod_{(n,\mu)\in\mathcal{P}} U_\mu(n) \right]. \tag{2.64}$$

The shortest non-trivial closed loop on the lattice is the plaquette, which is defined as a product of four link variables

$$\begin{aligned} U_{\mu\nu}(n) &= U_\mu(n)U_\nu(n+\hat{\mu})U_{-\mu}(n+\hat{\mu}+\hat{\nu})U_{-\nu}(n+\hat{\nu}) \\ &= U_\mu(n)U_\nu(n+\hat{\mu})U_\mu^\dagger(n+\hat{\nu})U_\nu^\dagger(n). \end{aligned} \tag{2.65}$$

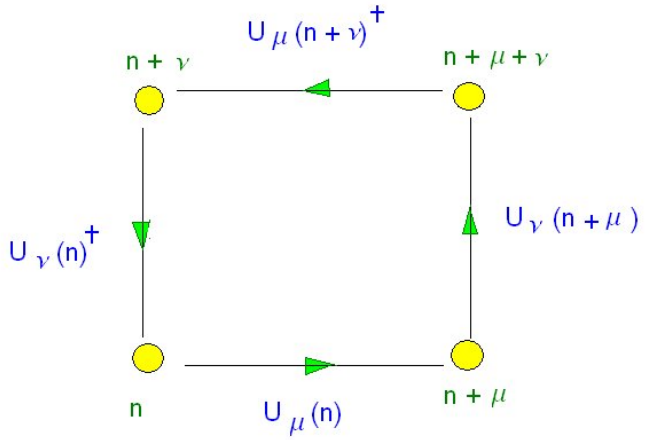

Figure 2.2: The plaquette is a product of 4 link variables around a closed loop. It is the simplest non-trivial closed loop, which can be constructed.

The trace of this product is gauge invariant. Inserting the explicit definition of link variables results in

$$U_{\mu\nu}(n) = \exp\left(iaA_\mu(n)\right)\exp\left(iaA_\nu(n+\hat{\mu})\right)\exp\left(-iaA_\mu(n+\hat{\nu})\right)\exp\left(-iaA_\nu(n)\right). \quad (2.66)$$

The Baker-Campbell-Hausdorff formula for the product of exponentials of matrices

$$\exp(A)\exp(B) = \exp(A + B + \frac{1}{2}[A,B] + ...) \quad (2.67)$$

can be applied to the intermediate result

$$\begin{aligned} U_{\mu\nu}(n) &= \exp(iaA_\mu(n) + iaA_\nu(n+\hat{\mu}) - \frac{a^2}{2}[A_\mu(n), A_\nu(n+\hat{\mu})] \\ &- iaA_\mu(n+\hat{\nu}) - iaA_\nu(n) - \frac{a^2}{2}[A_\mu(n+\hat{\nu}), A_\nu(n)] \\ &+ \frac{a^2}{2}[A_\nu(n+\hat{\mu}), A_\mu(n+\hat{\nu})] + \frac{a^2}{2}[A_\mu(n), A_\nu(n)] \\ &+ \frac{a^2}{2}[A_\mu(n), A_\mu(n+\hat{\nu})] + \frac{a^2}{2}[A_\nu(n+\hat{\mu}), A_\nu(n)] + \mathcal{O}(a^3)). \end{aligned} \quad (2.68)$$

In the next step a Taylor expansion of the fields

$$A_\nu(n+\hat{\mu}) = A_\nu(n) + a\partial_\mu A_\nu(n) + \mathcal{O}(a^2) \quad (2.69)$$

is exploited for simplification

$$\begin{aligned} U_{\mu\nu}(n) &= \exp\left(ia^2(\partial_\mu A_\nu(n) - \partial_\nu(n) + ia\left[A_\mu(n), A_\nu(n)\right]) + \mathcal{O}(a^3)\right) \\ &= \exp\left(ia^2 F_{\mu\nu}(n) + \mathcal{O}(a^3)\right). \end{aligned} \quad (2.70)$$

The exponential can be expanded:

$$U_{\mu\nu}(n) = \mathbb{1} + ia^2 F_{\mu\nu}(n) + \mathcal{O}(a^3) - \frac{1}{2}a^4 F_{\mu\nu}^2(n) + \mathcal{O}(a^6). \tag{2.71}$$

The terms $ia^2 F_{\mu\nu}(n)$ and $\mathcal{O}(a^3)$ in (2.71) disappear when taking the real part of the trace of the plaquette. Just the term $\mathcal{O}(a^4)$ remains. So we can make use of the plaquette to define the so-called Wilson's lattice gauge action

$$\begin{aligned} S_G[U] &= \frac{2}{g^2}\sum_{n\in\Lambda}\sum_{\mu<\nu}\text{Re tr}\left[1 - U_{\mu\nu}(n)\right] \\ &= \frac{a^4}{2g^2}\sum_{n\in\Lambda}\sum_{\mu<\nu}\text{tr}\left[F_{\mu\nu}(n)^2\right]. \end{aligned} \tag{2.72}$$

So far we have derived the lattice version of the fermion and gauge action. The whole action is

$$\begin{aligned} S &= S_F[\psi,\overline{\psi},U] + S_G[U] \\ &= a^4\sum_{n\in\Lambda}\overline{\psi}(n)\left(\sum_{\mu=1}^{4}\gamma_\mu\frac{U_\mu(n)\psi(n+\hat{\mu}) - U_{-\mu}(n)\psi(n-\mu)}{2a} + m\psi(n)\right) \\ &+ \frac{2}{g^2}\sum_{n\in\Lambda}\sum_{\mu<\nu}\text{Re tr}\left[\mathbb{1} - U_{\mu\nu}(n)\right]. \end{aligned} \tag{2.73}$$

We can insert this action into the definition of the two point function and obtain

$$\langle O_2(t)O_1(0)\rangle = \frac{\int\mathcal{D}[\psi,\overline{\psi}]\mathcal{D}[U]e^{-S_F[\psi,\overline{\psi},U]-S_G[U]}O_2[\psi,\overline{\psi},U]O_1[\psi,\overline{\psi},U]}{\int\mathcal{D}[\psi,\overline{\psi}]\mathcal{D}[U]e^{-S_F[\psi,\overline{\psi},U]-S_G[U]}} \tag{2.74}$$

and the equivalent expression for the observable

$$\langle O\rangle = \frac{\int\mathcal{D}[\psi,\overline{\psi}]\mathcal{D}[U]e^{-S_F[\psi,\overline{\psi},U]-S_G[U]}O[\psi,\overline{\psi},U]}{\int\mathcal{D}[\psi,\overline{\psi}]\mathcal{D}[U]e^{-S_F[\psi,\overline{\psi},U]-S_G[U]}}. \tag{2.75}$$

The denominator of these expressions is often referred to as partition function because of the similarity to statistical mechanics. The implementation of the QCD in the path integral formalism is implemented as an integral over all field configurations. The path integral measures are products of measures of all quark field components and products of measures for all link variables

$$\mathcal{D}[\psi,\overline{\psi}] = \prod_{n\in\Lambda}\prod_{f,\alpha,c}d\psi^{(f)}(n)_{\alpha,c}d\overline{\psi}^{(f)}(n)_{\alpha,c} \quad , \quad \mathcal{D}[U] = \prod_{n\in\Lambda}\prod_{\mu=1}^{4}dU_\mu(n). \tag{2.76}$$

Fermions fields underlie the Pauli principle, therefore the spinors can be seen as anti-commuting variables referred to Grassmann numbers and the Grassmann numbers have their specific integration rules. On the other side the integral measure for the gauge fields denoted in the measure $dU_\mu(n)$ can be seen as Haar measure, which describes the integration over a group [9].

2.3.3 Grassmann Integration

As mentioned, fermionic fields are not ordinary numbers, therefore the exponentiated fermionic action cannot be regarded as a probability. Instead the ψ and $\overline{\psi}$ are anti-commuting variables the so-called Grassmann variables

$$\{\psi_i, \psi_j\} = 0, \{\overline{\psi}_i, \overline{\psi}_j\} = 0, \{\overline{\psi}_i, \psi_j\} = 0. \tag{2.77}$$

Now we want to discuss the integration over anti-commuting variables. The measures obey

$$d\psi_i d\overline{\psi}_j = -d\overline{\psi}_j d\psi_i, \tag{2.78}$$

$$\int d\psi_i = 0 \quad , \quad \int d\psi_i \psi_i = 1. \tag{2.79}$$

A transformation of the measure produces

$$\begin{aligned} \int d^N\psi \ \psi_1\psi_2\dots\psi_N &= \int d^N\psi \ \psi'_1\psi'_2\dots\psi'_N \\ &= \det[M] \int d^N\psi' \ \psi_1\psi_2\dots\psi_N. \end{aligned} \tag{2.80}$$

All these relations can be used to derive formulas for Gaussian integrals with Grassmann numbers. One of the most famous formula is the Matthews-Salam formula

$$\int d^N\psi d^N\overline{\psi} \exp\left(\sum_{i,j}^{N} \overline{\psi}_i M_{ij} \psi_j\right) = \det[M]. \tag{2.81}$$

The application of the Matthews-Salam formula converts a partition function to an integral over ordinary numbers

$$\begin{aligned} Z &= \int \mathcal{D}[\psi,\overline{\psi}]\mathcal{D}[U] e^{-S_F[\psi,\overline{\psi},U]-S_G[U]} \\ &= \int \mathcal{D}[\psi,\overline{\psi}]\mathcal{D}[U] e^{-\overline{\psi}M[U]\psi-S_G[U]} \\ &= \int \mathcal{D}[U] \det[M] e^{-S_G[U]}. \end{aligned} \tag{2.82}$$

This is now an integral over numbers, therefore in principle accessible to Monte Carlo attack if $\det M \geq 0$. Because of the large size of the matrix M, it is not possible to solve it directly with Monte Carlo methods. The matrix M has the dimension of lattice sites times Dirac components times the number of internal (e.g., color) degrees of the freedom. There are many ways to deal with the fermion determinant [9, 10].

2.3.4 Haar Measure

Now we want to discuss the integration over a group. To do this we observe that a gauge transformation of the link variables (2.57) leaves the gauge action invariant

$$S_G[U'] = S_G[U]. \tag{2.83}$$

This fact also implies that the path integral should be invariant under the transformation of the link variables

$$Z = \int \mathcal{D}[U] e^{-S_G[U]} = \int \mathcal{D}[U'] e^{-S_G[U']} = \int \mathcal{D}[U'] e^{-S_G[U]} \tag{2.84}$$

and consequently we can extract from this equation the statement

$$\mathcal{D}[U] = \mathcal{D}[U']. \tag{2.85}$$

So we got a gauge invariant measure. For compact groups the measure is gauge invariant and satisfies

$$dU = d(UV) = d(VU), \tag{2.86}$$

where V is an arbitrary element of the group. These can be used to define some properties of the group measure or so-called Haar measure

$$\int dU f(U) = \int dU f(UV) = \int dU f(VU), \tag{2.87}$$

where $f(U)$ is an arbitrary function over the group. Additionally the measure is normalized such that

$$\int dU \mathbb{1} = 1. \tag{2.88}$$

In $\int dU f(U)$ only the gauge invariant contributions of $f(U)$ may contribute to the result This completes the definition of the lattice gauge theory [9, 10]. In the next section we will show how a lattice simulation of such a gauge theory is done.

3 LATTICE SIMULATION OF SU(3) GAUGE THEORY

3.1 Pure Gauge Theory

3.1.1 Introduction to SU(N) Pure Gauge Theory

As an example we are going to do a Monte Carlo simulation for the pure SU(2) gauge theory. The continuum gauge action is defined as

$$S_G[A] = \frac{1}{2g^2}\int dx^4 \mathrm{tr}\left[F_{\mu\nu}(x)F_{\mu\nu}(x)\right]. \tag{3.1}$$

For SU(N) gauge theory the discretized lattice gauge action (the so-called Wilson action) is given by

$$S_G[U] = \frac{\beta}{N}\sum_{n\in\Lambda}\sum_{\mu<\nu}\mathrm{Re\ tr}\left[\mathbb{1} - U_{\mu\nu}(n)\right] \tag{3.2}$$

with $U_{\mu\nu}(n)$ the plaquette which is defined as

$$\begin{aligned} U_{\mu\nu}(x) &= U_\mu(x)U_\nu(x+\hat{\mu})U_{-\mu}(x+\hat{\mu}+\hat{\nu})U_{-\nu}(x+\hat{\nu}) \\ &= U_\mu(x)U_\nu(x+\hat{\mu})U_\mu^\dagger(x+\hat{\nu})U_\nu^\dagger(x). \end{aligned} \tag{3.3}$$

This is the Wilson action which we have derived in the last section with the substitution

$$\beta = \frac{6}{g^2}. \tag{3.4}$$

The expectation value of an operator in a quantized Euclidean gauge field theory on lattice is given by the functional integral

$$\langle O\rangle = \frac{1}{Z}\int D\left[U\right] e^{-S_G[U]} O\left[U\right] \tag{3.5}$$

with

$$Z = \int D\left[U\right] e^{-S_G[U]}. \tag{3.6}$$

In a Monte Carlo simulation this integral is approximated by a sum of gauge configurations generated with the probability

$$P[U] = \frac{1}{Z}e^{-S[U]} = \frac{e^{-S[U]}}{\int dU e^{-S[U]}} \tag{3.7}$$

and then measuring

$$\bar{O} = \frac{1}{N}\sum_{i=0}^{N} O[U_i] \quad , \quad \sigma_0^2 = \frac{1}{N-1}\sum_{i=0}^{N}\left(O[U_i] - \bar{O}\right)^2 \tag{3.8}$$

on a Markov sequence of such configurations U_i. The observable with its error is given by

$$\langle O \rangle \quad = \quad \bar{O} + \frac{\sigma}{\sqrt{N}}. \tag{3.9}$$

To compute the observables sufficiently many such configurations are needed.

3.1.2 Generation of the Configurations

In general it is important to generate configurations with the desired distribution. An effective approach for this generation is by a Markov process. A Markov process is a stochastic procedure. The new generated configuration depends only on the configuration, which was generated before. Any Markov process converges to a fixed point distribution and it is ergodic. The construction of a Markov process is done by important sampling.

3.1.3 Important Sampling

In this approach one has to sample configurations U weighted according to the probability given by the Boltzmann factor

$$P[U] \propto \exp(-\beta S[U]), \tag{3.10}$$

where $S[U]$ is the action functional of the configuration U. This probability distribution has many local maxima and the location of peaks in configuration space is unknown. Important sampling helps to find a sequence of configurations which are distributed according to the given probability density. This sequence of configurations is a Markov chain. A Markovian process is a process where the next step depends only on the step before.

In other words, each configuration is generated from the configuration before through a random process with a transition probability

$$W(U \to U') \quad = \quad W(U^{t+1} = U' | U^t = U) \tag{3.11}$$

with its properties $0 \leq W(U \to U') \leq 1$ and $\sum_{U'} W(U \to U') = 1$.

The transitions should lead after some equilibration steps to a configuration distributed according to $P[U]$. In equilibration one can formulate a balance equation

$$\sum_{U} P[U] W(U \to U') \quad = \quad \sum_{U} P[U'] W(U' \to U). \tag{3.12}$$

The left side of this equation counts the total probability to arrive in a Markov step at U' and the right side gives the total probability to leave U in a step. If one uses the property $\sum_{U'} W(U \to U') = 1$ of the transition probability one gets

$$\sum_{U} P[U]W(U \to U') \quad = \quad P[U']. \tag{3.13}$$

This equation is a fixed point equation. $P[U]$ is the fixed point distribution under the transition sequence. So it is the fixed point of the Markov chain. Under certain general assumptions one can show that the fixed point is attractive. It means that the Markov process approaches the desired distribution $P[U]$ and the balance equation is still fulfilled. A sufficient condition to satisfy the balance equation is the so-called detailed balance equation

$$P[U]W(U \to U') \quad = \quad P[U']W(U' \to U). \tag{3.14}$$

One of the widely-used algorithms which give a possible solution of the detailed balance equation is the Metropolis algorithm [9].

3.1.4 Metropolis Algorithm

The algorithm is named after Nicholas Metropolis who was an author of a seminar article along with Arianna W. Rosenbluth, Augusta H.Teller and Edward Teller [11]. It was the first proposed algorithm for a specific case of the Boltzmann distribution. It was extended to a more general case by W. Keith Hastings in 1970 [12]. It is used to produce the configurations according the Boltzmann distribution. The algorithm proceeds as follows:

(1) One starts from a configuration U. This could be a cold start, a hot start or a mixture of both. Cold start means that all variables have the same value. Hot start means that one starts from a disordered random configuration.

(2) Generate a new configuration $\tilde{U}$ near the old configuration U

(3) Calculate $\rho = \frac{P[\tilde{U}]}{P[U]} \in [0, \infty)$

(4) Compute a random number $r \in [0, 1]$
   a) if $\rho \geq r$ accept $\tilde{U}$ as the new configuration $\tilde{U} \to U^{t+1}$
   b) if $\rho < r$ keep the old configuration $U \to U^{t+1}$

(5) $t \to t + 1$ go to (2)

Next we will discuss a Monte Carlo simulation of SU(2) using the Metropolis algorithm.

3.2 Monte Carlo Simulation of Pure Gauge Theory

3.2.1 SU(2) Pure Gauge Theory

We consider a 4 dimensional lattice.

$$x = (x_1, x_2, x_3, x_4),$$

i.e.

$$\begin{aligned} x_1 &= 0, 1, ...L-1, \\ x_2 &= 0, 1, ...L-1, \\ x_3 &= 0, 1, ...L-1, \\ x_4 &= 0, 1, ...L-1. \end{aligned}$$

The representations for the gauge field variables are complex 2×2 matrices for SU(2). The minimal number of parameters for SU(2) is the number of its generators: 3. It is good to use a redundant representation of the group to decrease the CPU time. For SU(2) it is convenient to store the first row (a, b) of the matrix

$$U = \begin{pmatrix} a & b \\ -b^* & a^* \end{pmatrix}. \tag{3.15}$$

In this case this corresponds storing two complex numbers, written as four real numbers. So one has 4 parameters instead of 3 parameters. We can use these 4 real parameters and the Pauli matrices to construct the SU(2) elements with the prescription

$$U = x_0 + i\vec{\sigma}\vec{x} \quad \text{with} \quad \det[U] = x_0^2 + |\vec{x}|^2 = \sum_{i=0}^{3} x_i^2 = 1 \tag{3.16}$$

where $\vec{\sigma}$ is the vector of 3 Pauli matrices and $(x_0, \vec{x})$ are 4 real parameters.

After the generation of the configurations within Metropolis algorithm [9, 13] we can now go on to calculate observables with these configurations. We consider the Wilson loops and how the confinement potential is extracted from these.

3.2.2 Wilson-Loops and Static Quark Potential

Wilson-loops are observables which allow us, e.g., to calculate the potential between two static color sources. They consist of four pieces: the two so-called Wilson-lines and two temporal transporters. Wilson-lines connect two spatial points along some path. In general we can write a planar Wilson-loop as

$$\begin{aligned} W^{\mu,\nu}_{m,n}(x) &= U_\mu(x)U_\mu(x+\hat{\mu})\dots U_\mu(x+(m-1)\hat{\mu}) \\ &+ U_\nu(x+m\hat{\mu})U_\nu(x+m\hat{\mu}+\hat{\nu})\dots U_\nu(x+m\hat{\mu}+(n-1)\hat{\nu}) \\ &+ U^\dagger_\mu(x+n\hat{\nu})U^\dagger_\mu(x+n\hat{\nu}-\hat{\mu})\dots U^\dagger_\mu(x+n\hat{\nu}+(m-1)\hat{\mu}) \\ &+ U^\dagger_\nu(x)U^\dagger_\nu(x-\hat{\nu})\dots U^\dagger_\nu(x+(n-1)\hat{\nu}). \end{aligned} \tag{3.17}$$

Averaging over all possibilities (for a given combination n, m),

$$W_{m,n} = \frac{1}{12V} \sum_x \sum_{\mu \neq \nu} \left\langle \text{Re Tr}[W^{\mu,\nu}_{m,n}(x)] \right\rangle, \tag{3.18}$$

we get the values of the average $m \times n$ planar Wilson loops. The next step is to calculate from the average Wilson loops the static quark potential. In temporal gauge we can set the two temporal transporters to identity. So we get in this case the Wilson loop as correlator of the two Wilson lines $S(m, n, n_t)$ and $S(m, n, 0)$ which can be written as

$$\begin{aligned} \langle W \rangle &= \left\langle \text{tr}[S(m,n,n_t) S(m,n,0)^\dagger] \right\rangle_{temp} \\ &= \sum_k \langle 0| \, S(m,n,n_t)_{ab} \, |k\rangle \, \langle k| \, S(m,n,0)^\dagger_{ba} \, |0\rangle \, e^{-a n_t E_k}. \end{aligned} \tag{3.19}$$

The term with lowest energy E_1 describes the state of static quark–anti-quark pair. The energy E_1 is the energy of the quark–anti-quark pair which corresponds to the static potential V(R).

$$E_1 = V(R) \quad \text{with} \quad R = a|m - n|. \tag{3.20}$$

So we get finally the result

$$< W_L > \approx e^{-n_t a V(R)} (1 + O(e^{-n_t a \Delta E})). \tag{3.21}$$

For large n_t the corrections are exponentially suppressed. We set $T = a n_t$. So the expression becomes

$$W(R, T) \approx e^{-TV(R)}. \tag{3.22}$$

From this relation we can get the potential through

$$V(R) = -\lim_{T \to 0} \frac{\ln(W(R,T))}{T}. \tag{3.23}$$

We can control this if we plot

$$\ln(W(R,T)) \approx -V(R)T. \tag{3.24}$$

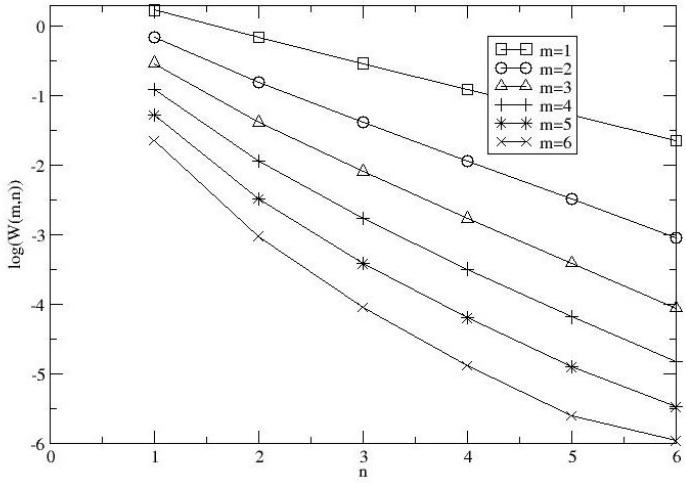

Figure 3.1: Logarithm of different Wilson loops plotted versus time. Up to the 6x6 Wilson loops are taken in account

From the slope of this straight lines we can construct the (confinement) potential:

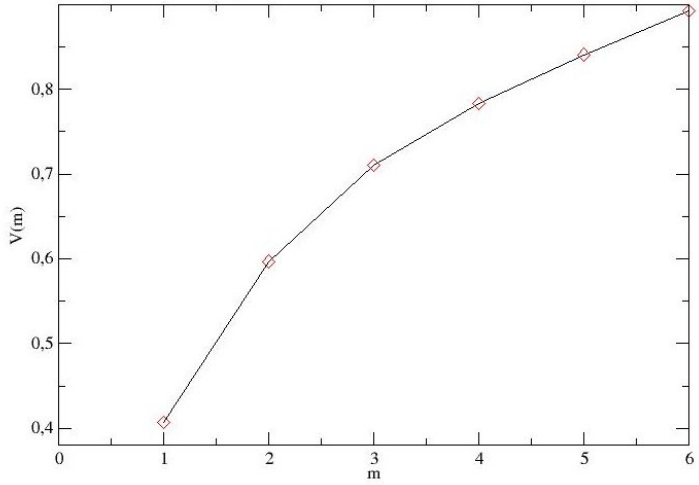

Figure 3.2: Confinement potential versus the distance.

From this figure we see the two regions of the potential. The one is the short distance non linear potential and the second part is long distance linear rising (confining) potential.

3.2.3 SU(3) Pure Gauge Theory

It is not necessary to repeat again the details, we will only consider the differences to the SU(2). The representation of SU(3) gauge field variables are 3×3 matrices. The minimal

number of parameters are 8 real numbers (the number of the generators). The group elements of SU(3) could be represented by the complete 3×3 complex matrices. That means 9 complex numbers corresponding to 18 real numbers instead of 8 real numbers. It is also possible to store only the first two rows and construct the third one orthogonal to the first two. Our SU(3) group element is then

$$U = \begin{pmatrix} & u & \\ & v & \\ u^* \times & v^* & \end{pmatrix}. \tag{3.25}$$

In this way we need to store 6 complex numbers corresponding to 12 real numbers. This is one of the main differences to SU(2). These 12 real numbers can be constructed from SU(2) matrices. In the Metropolis updating algorithm the updating matrices X can be constructed from SU(2) matrices in such a way that they are embedded in 3×3 matrices according to

$$R = \begin{pmatrix} r_{11} & r_{12} & 0 \\ r_{21} & r_{22} & 0 \\ 0 & 0 & 1 \end{pmatrix} \quad , \quad S = \begin{pmatrix} s_{11} & 0 & s_{12} \\ 0 & 1 & 0 \\ s_{21} & 0 & s_{22} \end{pmatrix}, T = \begin{pmatrix} 1 & 0 & 0 \\ 0 & t_{11} & t_{12} \\ 0 & t_{21} & t_{22} \end{pmatrix}. \tag{3.26}$$

So the updating matrix can be chosen by the product of these 3 matrices

$$X = RST. \tag{3.27}$$

Obviously to do this simulation, 3 different SU(2) updating steps are necessary for each SU(3) element [9].

3.3 SU(3) Gauge Theory

3.3.1 Introduction to SU(3) Gauge Theory

In the section above we dealed with the lattice simulation of a pure gauge theory. In the language of Quantum Chromodynamics we consider only gluon fields. If we include the quark fields the simulation becomes more complicate, because the quark fields are Grassmann variables. The action is (2.73), i.e.,

$$\begin{aligned} S &= S_F[\psi, \overline{\psi}, U] + S_G[U] \\ &= a^4 \sum_{n \in \Lambda} \overline{\psi}(n) \left(\sum_{\mu=1}^{4} \gamma_\mu \frac{U_\mu(n)\psi(n+\hat{\mu}) - U_{-\mu}(n)\psi(n-\mu)}{2a} + m\psi(n) \right) \\ &+ \frac{2}{g^2} \sum_{n \in \Lambda} \sum_{\mu < \nu} \mathrm{Retr}\left[\mathbb{1} - U_{\mu\nu}(n) \right]. \end{aligned}$$

The inclusion of the quark fields brings in the fermion determinant

$$\langle O \rangle = \frac{1}{Z} \int \mathcal{D}[U] \det[M] e^{-S_G[U]} O[U], \tag{3.28}$$

where

$$Z = \int \mathcal{D}[U] \det[M] e^{-S_G[U]}. \tag{3.29}$$

There are some problems to use Monte Carlo methods to approximate this integral. This is because in a Monte Carlo calculation each link variable interacts with its neighbors and a simultaneous update of all link variables would be unlikely to be accepted. This problem can be avoided by the so-called hybrid Monte Carlo algorithm.

3.3.2 Hybrid Monte Carlo Algorithm

The algorithm which combines the Molecular dynamics (the calculation of equation of motion method) with a Monte Carlo algorithm (for example, Metropolis algorithm) is called Hybrid Monte Carlo algorithm [14]. In Hamiltonian Molecular dynamics a new (computer) time variable τ is introduced. The Hamiltonian dynamics is used to specify the development of the configurations $U(\tau)$ in this time. The solution of this equations of motion gives the desired probability distribution for each field of the theory. Numerical integration schemes allow one to avoid the problem of non-locality. To do this we introduce conjugate momenta $P(\tau)$. The Hamiltonian becomes

$$H(U,P) = \frac{1}{2}P^2 + S[U] \tag{3.30}$$

where S is the action. From this Hamiltonian we can construct the following equations of motion

$$\dot{U} = \frac{\partial H}{\partial P} = P, \tag{3.31}$$

$$\dot{P} = -\frac{\partial H}{\partial U} = -\frac{\partial S}{\partial U}. \tag{3.32}$$

Our procedure for generating a new configuration U' is to select some initial momenta P at random from a Gaussian distribution of mean zero and unit variance

$$P_G(P) \propto e^{-\frac{P^2}{2}} \tag{3.33}$$

and let the system evolve deterministically through (U,P) space for a fixed τ_0 according the Hamiltonians equations. For the integration of the Hamiltonian equations the so-called leapfrog algorithm can be used. The initial half step is

$$\begin{aligned} P(\frac{\delta\tau}{2}) &= P(0) - \dot{P}(0)\frac{\delta\tau}{2} \\ &= P(0) - \frac{\partial S(0)}{\partial U}\frac{\delta\tau}{2}. \end{aligned} \tag{3.34}$$

This step is followed by $n = \tau_0/\delta\tau$ steps in U and n-1 steps in P which have the form

$$U(\tau + \delta\tau) = U(\tau) + P(\tau + \frac{\delta\tau}{2}) \cdot \delta\tau \tag{3.35}$$

$$P(\tau + \frac{\delta\tau}{2}) = P(\tau - \frac{\delta\tau}{2}) - \frac{\delta S(\tau)}{\delta U}\delta\tau. \tag{3.36}$$

The final half step has the form

$$P(\tau_0) = P(\tau_0 - \frac{\delta\tau}{2}) - \frac{\delta S(\tau_0)}{\delta U}\delta\tau. \tag{3.37}$$

Through the solution of Hamiltonian equations we get a phase space trajectory in computer time. This new generated phase space trajectory (U', P') is accepted with probability:

$$P((U, P) \to (U', P')) = \min(1, e^{-\Delta H}) \tag{3.38}$$

where

$$\Delta H = H(U', P') - H(U, P). \tag{3.39}$$

Summarizing one can write the following steps of Hybrid Monte Carlo algorithm

(1) Assume U is the starting configuration

(2) We generate a momentum P at random from Gaussian distribution according to (3.33)

(3) For a fixed τ we let (U, P) evolve according to the Hamiltonian equations

(4) Calculate the energy difference ΔH in phase space

(5) Generate a random number $r \in [0, 1)$:
   a) if $r < e^{-\beta\Delta H}$ accept $\tilde{U}$ as the new configuration $\tilde{U} = U^{t+1}$
   b) else keep the old configuration $U = U^{t+1}$

3.3.3 HMC Algorithm for SU(3) Gauge Theory

The challenge now is to implement the hybrid Monte Carlo algorithm for the SU(3) gauge theory. The partition function for lattice gauge theory is given by

$$\begin{aligned} Z &= \int \mathcal{D}[\psi, \overline{\psi}]\mathcal{D}[U]e^{-\overline{\psi}M[U]\psi - S_G[U]} \\ &= \int \mathcal{D}[U](\det[M])^{N_f}e^{-S_G[U]}. \end{aligned} \tag{3.40}$$

For simplicity we set $N_f = 2$ (this ensures that $(\det M)^2 \geq 0$) and assume mass generate quarks. The prescription to calculate an observable is

$$\langle O \rangle = \frac{1}{Z}\int \mathcal{D}[U]e^{-S_G[U]}\det(M[U]^2)O[U]. \tag{3.41}$$

This corresponds to generating the gauge configurations with the probability factor

$$P[U] = e^{-S_G[U]}\det(M[U]^2). \tag{3.42}$$

Some problem appears in this stop because of the determinant which leads to a non-local action. The remedy of this problem is Hybrid Monte Carlo algorithm where global updates are possible because of the numerical integration of equation of motion and the truncation errors are eliminated by a Monte Carlo step. To implement it we replace the fermionic fields ψ and $\overline{\psi}$ by bosonic fields χ^* and χ with non-local interactions

$$Z = \int \mathcal{D}\chi^*\mathcal{D}\chi\mathcal{D}[U]e^{-\chi^*(M^\dagger M)^{-1}\chi - S_G[U]}. \tag{3.43}$$

This is the so-called pseudo–fermion method [15, 16]. Our effective action is now

$$S_{\text{eff}} = S[U] + \chi^*(M^\dagger M)^{-1}\chi. \tag{3.44}$$

To calculate the equations of motion we want construct the Hamiltonian. Therefore we introduce an fictitious time τ. The gauge field is associated with its fictitious conjugate momenta P_μ. The Hamiltonian which describes this system is

$$H[U,P] = \sum_{x,\mu}\frac{1}{2}\text{tr}\left(P_\mu(x)^2\right) + S_{\text{eff}}[U]. \tag{3.45}$$

If we select the conjugate momenta Gaussian distributed then the expectation value of an observable is uneffected by the momenta

$$\langle O\rangle = \frac{1}{Z}\int \mathcal{D}P\mathcal{D}[U]O[U]e^{-H[U,P]}, \tag{3.46}$$

$$Z = \int \mathcal{D}P\mathcal{D}[U]e^{-H[U,P]}. \tag{3.47}$$

It is not necessary to go through every step again instead we give the important steps to generate a new gauge configuration U' from a given gauge configuration U:

(1) Start with an initial configuration U. Sample the conjugate momenta P according the Gaussian ensemble $P_G(P) = e^{-\frac{1}{2}\text{tr}(P^2)}$. Then generate the pseudo fermionic fields χ by applying the Fermion operator on a complex, Gaussian distributed vector η: $M\eta = \chi$

(2) Molecular Dynamics trajectory: Integrate the Hamiltonian equations of motion using for example using leapfrog algorithm to evolve (U,P) along a phase space trajectory to (U',P').

(3) Monte Carlo Step: Accept or reject a new configuration (U',P') with probability $P(U\to U') = \min(1, e^{-\Delta H})$.

In this way the gauge fields are updated according to $e^{-S_{\text{eff}}}$. We have mentioned that the Hamiltonian equations of motion are solved with the leapfrog algorithm. We can give the solutions for small step sizes $\Delta\tau$ in following way

$$U_\mu(x, x + \Delta\tau) = U_\mu(x, \tau)e^{i\Delta\tau P_\mu(x,\tau)}, \tag{3.48}$$

$$P_\mu(x, x + \Delta\tau) = P_\mu(x, \tau) - U_\mu(x, \tau)\frac{\delta S_{\text{eff}}}{\delta U_\mu(x, \tau)}. \tag{3.49}$$

Matrix exponentials can be evaluated directly by diagonalization. We see also the variation of the action with respect to the link variables. In the HMC algorithm also link smearing can be used but it is necessary that the smearing method is differentiable. With this algorithm and some numerical ability one can generate the configurations. The gauge configurations use here have been constructed with similar methods in [14, 17, 18]. In the next section we will treat some commonly used smearing methods.

4 MOST COMMON SMEARING METHODS

4.1 Introduction to Smearing

Quantum field configurations at short distances fluctuate wildly. They are continuous but not differentiable. The general idea of a smearing procedure is to reduce these short distance fluctuations [19, 20].

The smearing procedure is a transformation. This transformation averages the products of link variables along certain paths connecting the endpoint of a link. The link variables are then replaced by the weighted average of such variables. In this way short distance (wavelength) fluctuations are suppressed. Smearing algorithms are used much in lattice gauge theory. Through smearing algorithms operators are constructed which have better chiral symmetry and flavor symmetry behavior [21].

The extraction of hadron masses and matrix elements from Monte Carlo estimates of Euclidean space correlation functions in lattice QCD can be done better when operators which couple more strongly to the states of interest and less strongly to higher-lying contaminating states are used. For states which contain gluons such operators are constructed using smeared link variables. The use of such operators gives better results in the determination of glueball spectrum, baryon masses, hybrid meson masses the excitations of the static quark–anti-quark potential [22].

Also better results are obtained in the study of 3 quark potential, which is extracted from 3 quark Wilson-loop. For large T excited state component decreases faster than the ground state, however the ground state component also decreases exponentially. Smearing methods enhances the ground state overlap and suppress the excited state contamination efficiently [23].

In literature the names fat links and thin links appear. Fat links are the smeared links and thin links are the original links. In the Wilson formulation it is difficult to simulate light quark masses because of the violation of the chiral symmetry. This leads to arbitrarily small eigenvalues for Dirac operator and may lead to spurious zero modes for individual configurations. This is the so-called problem of exceptional configurations, which leads to convergence difficulties for the fermion matrix inversion. Fermion matrix inversion is important for the generation of gauge configurations with dynamical fermions. So another benefit of smearing algorithms is that through smearing fat links are constructed and the action based on the fat link variables has better chiral behavior and reduced exceptional configuration problems. Its gauge action has reduced discretization errors [24, 22].

Such gauge actions are often called UV-filtered actions [25]. In lattice gauge theory there is also a flavor symmetry breaking with staggered fermions. This is because of the distribution of Dirac spinors components to different lattice sites. Consequently

since each lattice site couples to different gauge fields, the different flavor and Dirac components interact with different gauge surroundings. Smearing improves the flavor symmetry [26].

As mentioned smearing reduces the noise but also for (not too) many steps of smearing the IR structures are not altered by the smearing method. Fermionic observables do not appreciably alter in a sequence of smoother and smoother configurations. But if any smearing transformation is repeated enough times, this would eventually wash away vacuum structures [27, 28].

Some smearing procedures lead out of the gauge group SU(3). So it is necessary to project the smeared links back to the gauge group SU(3). There are many ways to do such a projection. In a projection back to SU(3) a kind of maximization procedure is used. This way of projection is an arbitrary and abrupt way to stay within the group and therefore not differentiable. The lack of differentiability makes it impossible to applicate the Hybrid Monte Carlo updating technique, which requires knowing the response of the action to a small change of the link variables.

Summarizing, in general there are two steps of a smearing algorithm. These are:

(a) Calculation of a variable $\tilde{U}'_\mu(n)$ as a function of the old link variable and neighbored link variables $U_\mu(n)$: $\tilde{U}'(U)$

(b) Unitarization of the new link variable $\tilde{U}'_\mu(n)$. That means mapping the smeared new link variable $\tilde{U}'_\mu(x)$ back to the original link variable $U_\mu(n)$

These two steps define a smearing step or smearing sweep, which can be iterated.

Now we will go through some of the most important and most used smearing methods. The first proposed smearing method is APE smearing. It was proposed by M. Albanese and others in APE Collaboration [20]. Because of the lack of differentiability which is necessary for HMC algorithm, C. Morningstar and M. Peardon invented STOUT smearing [22]. STOUT smearing yields differentiable fat links but is less effective than APE smearing in the damping of the UV fluctuations. Consequently a modified version of APE smearing so-called n-APE smearing was invented by A. Hasenfratz, R. Hoffmann and S. Schaefer, where the projection to SU(3) is replaced by U(3) to obtain the differentiability [29].

In the next step the attempt to reach a more effective smearing and fat links with better properties HYP smearing was invented by A. Hasenfratz, R. Hoffmann and F. Knechtli [26]. In HYP smearing gauge configurations are smoothed within a hypercube. The disadvantage of this method is that it is not differentiable like in APE smearing. The differentiable version of HYP smearing is the n-HYP smearing [30]. One of the recently invented smearing methods is logarithmic link smearing with hypercubic nesting trick abbreviated LOG/HYL smearing [31]. These are the most important smearing methods. For our consideration we will study APE smearing, HYP smearing, n-HYP smearing and STOUT smearing. Therefore we will discuss these methods in more detail. Before that it is useful to study the 2nd step of the smearing algorithm referred to as projection back to SU(3).

4.2 Projection to SU(3)

The necessity of projection back to SU(3) results from the way of constructing the smearing method. In some cases smearing leads out of the group SU(3). We want to study the details of such a projection. To see it more transparent we first look at such a projection for the SU(2) gauge group. We assume that the new link variable $\tilde{U}'$ is constructed by any of the smearing methods which lead out of the gauge group, i.e., the smeared link variable $\tilde{U}'$ is a sum of gauge variables. Since the sum of SU(2) elements is proportional to SU(2) elements

$$\tilde{U}'_\mu(n) \quad = \quad k\overline{U}_\mu(n), \tag{4.1}$$

where $\overline{U}_\mu(n) \in SU(2)$ and

$$k^2 \quad = \quad \det\left(\tilde{U}'_\mu(n)\right). \tag{4.2}$$

The expression Re tr$[\mathbb{1} - U_\mu(n)\tilde{U}'_\mu(n)]$ is minimized if the term Re tr$[U_\mu(n)\tilde{U}'_\mu(n)]$ is maximized. Because of the argument that the sum of SU(2) elements is proportional to the SU(2) elements we can write this term as

$$\text{Re tr}[U_\mu(n)\tilde{U}'_\mu(n)] = \text{Re tr}[kU_\mu(n)\overline{U}_\mu(n)]. \tag{4.3}$$

The maximization of this expression is achived when

$$\text{Re tr}[U_\mu(n)\overline{U}_\mu(n)] = \text{Re tr}[\mathbb{1}]. \tag{4.4}$$

So using this two expressions we get as our final result

$$\overline{U}_\mu(n)^{-1} = \overline{U}_\mu(n)^\dagger = \frac{(\tilde{U}'_\mu(n))^\dagger}{k}. \tag{4.5}$$

For SU(3) one has to apply this procedure to the three SU(2) subgroups of SU(3) to cover the whole SU(3) gauge group [32, 33].

The standard procedure for projecting the new links $\tilde{U}'_\mu(n)$ back to SU(3) is defined by

$$\begin{aligned} \text{Proj}_{SU3}(U'_\mu(n)) \quad &= \quad U_\mu(n) \\ &= \quad \max_{U_\mu(n)\in SU(3)} \text{Re tr}(U_\mu(n)\tilde{U}'_\mu(n)^\dagger), \end{aligned} \tag{4.6}$$

where U' is sum of SU(3) matrices and thus it is not a SU(3) matrix itself. The projection is finished if the matrix U is found, which maximizes the above relation. It can be found by an iterative process [21, 22, 34]. Another opportunity to do the projection back to SU(3) can be written as [35]:

$$U \quad = \quad \tilde{U}'(\tilde{U}'^\dagger\tilde{U}')^{-1/2}\det(\tilde{U}'^{-1}\tilde{U}'^\dagger)^{1/6}, \tag{4.7}$$

where we have left out the indices for simplicity. This relation can be obtained by starting with any matrix $\tilde{U}'$, then $\tilde{U}'^{\dagger}\tilde{U}'$ is Hermitian and may be diagonalized. For $\det(\tilde{U}') \neq 0$ it is possible to calculate

$$W = \tilde{U}' \frac{1}{\sqrt{\tilde{U}'^{\dagger}\tilde{U}}}. \tag{4.8}$$

The spectrum of W lies on the complex unit circle and hence it is unitary. From W we can construct another matrix

$$U = W \frac{1}{\sqrt[3]{\det W}}, \tag{4.9}$$

which is special unitary and is exactly (4.7). Inserting (4.8) in (4.9) it can simply verified. Obviously projections to the SU(3) are not unique .

4.3 APE-Smearing

One of the earliest introduced smearing methods is APE smearing [20]. In APE smearing a link variable $U_\mu(n)$ is substituted by a combination with neighboring stables. The linear combination is

$$\tilde{U}'_\mu(n) = (1-\alpha)U_\mu(n) + \frac{\alpha}{6}\sum_{\mu\neq\nu} C_{\mu\nu}(n), \tag{4.10}$$

where

$$\begin{aligned} C_{\mu\nu}(n) &= U_\nu(n)U_\mu(n+\hat{\nu})U_\nu^\dagger(n+\hat{\mu}) \\ &+ U_\nu^\dagger(n-\hat{\nu})U_\mu(n-\hat{\nu})U_\nu(n-\hat{\nu}+\hat{\mu}). \end{aligned} \tag{4.11}$$

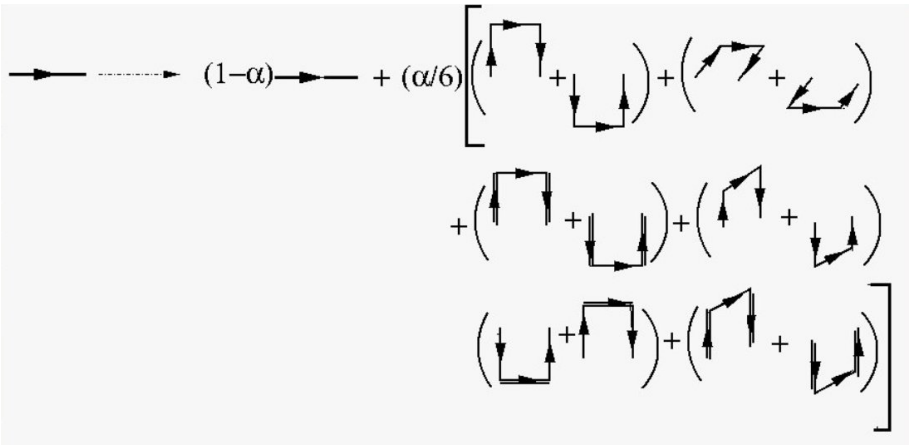

Figure 4.1: Ape smearing procedure; A link is substituted by $(1-\alpha)$ multiplied by itself and α times the average of the staples. At the end of this procedure the new link should be projected back to SU(3).

The symbol α represents the smearing fraction. It is an adjustable parameter. The calculated new link variable is projected back to the SU(3). In the previous section we have discussed the projection back to SU(3). For example, this projection back to SU(3) could be because of the non uniqueness of the projection

$$\begin{aligned} \mathrm{Proj}_{SU3}(\tilde{U}'_\mu(n)) &= \max \mathrm{Re\ tr}(U_\mu(n)\tilde{U}'^\dagger_\mu(n)) \\ &= \max \mathrm{Re\ tr}(U_\mu(n)(1-\alpha)U^\dagger_\mu(n) + \frac{\alpha}{6}\sum_{\mu\neq\nu} C^\dagger_{\mu\nu}(n)). \end{aligned} \tag{4.12}$$

Finally we want to comment on the APE smearing. Smearing can be also understand in another way. We can say that it is like introducing a form factor which is suppressing the coupling of gluons to the quarks at the edge of the Brillouin zone where the lattice artifacts are the most problematic. The form factor analysis restricts the smearing parameter to the range $0 \leq \alpha \leq 3/4$. Beyond 3/4 APE smearing does not lead to smooth gauge configurations [36].

This can be tested if one smears the plaquette for different parameters. The plaquette increases for small parameter α reachs a maximum around $\alpha = 0.7$ then it decreases again. This holds for larger loops too. Best parameter is $\alpha = 0.6$ [21, 37]. On the one side to reach smooth gauge configurations and on the other side to reach high damping of UV fluctuations we select our smear parameter α near the optimal value as

$$\alpha = 0.55 \tag{4.13}$$

4.4 HYP-Smearing

HYP smearing is the abbreviation for the name hypercubic smearing [26]. In HYP smearing the gauge configurations are smoothed within an hypercube sized volume but not beyond it.

The smeared link variables (fat links) of hypercubic blocking are constructed in three steps. The first step is:

$$\begin{aligned} \bar{V}_{\mu,\nu,\rho}(n) &= \mathrm{Proj}_{SU(3)}[(1-\alpha_3)U_\mu(n) \\ &+ \frac{\alpha_3}{2}\sum_{\eta\neq(\rho,\mu,\nu)} (U_\eta(n)U_\mu(n+\hat{\eta})U^\dagger_\eta(n+\hat{\mu}) \\ &+ U^\dagger_\eta(n-\hat{\eta})U_\eta(n-\hat{\eta})U_\mu(n-\hat{\mu}-\hat{\eta}))]. \end{aligned} \tag{4.14}$$

In the first step the two staples orthogonal to μ,ν and ρ are used.
The second step is:

$$\begin{aligned} \tilde{V}_{\mu,\nu}(n) &= \mathrm{Proj}_{SU(3)}[(1-\alpha_2)U_\mu(n) \\ &+ \frac{\alpha_2}{4}\sum_{\rho\neq(\nu,\mu)} (\bar{V}_{\rho,\nu\mu}(n)\bar{V}_{\mu,\rho\nu}(n+\hat{\rho})\bar{V}^\dagger_{\rho,\nu\mu}(n+\hat{\mu}) \\ &+ \bar{V}^\dagger_{\rho,\nu\mu}(n-\hat{\rho})\bar{V}_{\mu,\rho\nu}(n-\hat{\rho})\bar{V}_{\rho,\nu\mu}(n+\hat{\mu}-\hat{\rho}))], \end{aligned} \tag{4.15}$$

where the indices ρ, μ indicate that the fat link $\bar{V}_{\mu,\rho\nu}(n)$ in direction μ is not decorated with staples extending in ρ and μ directions.
In the final step the blocked link is constructed via APE blocking from a set of decorated links $\tilde{V}_\mu(n)$ as

$$\begin{aligned} V_\mu(n) &= \mathrm{Proj}_{SU(3)}[(1-\alpha_1)U_\mu(n) \\ &+ \frac{\alpha_1}{6}\sum_{\nu\neq\mu}(\tilde{V}_{\nu,\mu}(n)\tilde{V}_{\mu,\nu}(n+\hat{\nu})\tilde{V}^\dagger_{\nu,\mu}(n+\hat{\mu}) \\ &+ \tilde{V}^\dagger_{\nu,\mu}(n-\hat{\nu})\tilde{V}_{\mu,\nu}(n-\hat{\nu})\tilde{V}_{\nu,\mu}(n+\hat{\mu}-\hat{\nu}))]. \end{aligned} \tag{4.16}$$

This construction allows that the fat link $V_\mu(n)$ mixes the thin links only from hypercubes attached to the original link. The parameters α_1, α_2 and α_3 can be optimized to achieve the smoothest block link configuration [26].

There are various ways to optimize the parameters of the hypercubic blocking. For example, for staggered fermions, one can use the level of the flavor symmetry restoration to optimize the parameters of the hypercubic blocking. But this method is very CPU time expensive, so one has to look for an easier method. Let us look at the reason for the flavor and chiral symmetry violation. The staggered fermions' flavor symmetry violation and Wilson fermions' exceptional configurations can be understood as fluctuations in the local plaquette. Few of the largest plaquette fluctuations create dislocations. In case to minimize the largest fluctuations we have to maximize the smallest plaquettes of the system. This is done by looking at the distribution of the smallest plaquette values on a finite, fixed volume. The point is that if we optimize the parameters α_1, α_2 and α_3 we will get largest expectation value for the smallest plaquette in this finite volume ensemble. The parameters α_1, α_2 and α_3 are optimized through using a set of 500 4^4 lattices created at $\beta = 5.7$ with the Wilson plaquette action. The final result for the parameters is [26]:

$$\alpha_1 = 0.75,\ \alpha_2 = 0.6 \quad \text{and} \quad \alpha_3 = 0.3. \tag{4.17}$$

An important point is that the plaquette values are maximized but not the average plaquette values.

One of the main advantages of the HYP smearing is that because it smears the gauge fields within an hypercube consequently this improves the flavor symmetry breaking of the staggered fermions [26].

4.5 n-HYP Smearing

The n-HYP smearing is very similar to HYP smearing. The only difference between n-HYP smearing and HYP smearing is the projection. In HYP smearing the projection is to SU(3) and in n-HYP smearing the projection is to U(3) [30]. So we can write the three steps of n-HYP smearing in consideration of this fact and define the n-HYP

smearing by using the equations (4.14), (4.15) and (4.16) with the replacement of the projection to U(3).

How is the projection to U(3) defined? Let us assume we have a 3×3 matrix A, which is non-singular. The projection of this operator to U(3) is defined by

$$\text{Proj}_{U(3)} A \quad = \quad A \frac{1}{\sqrt{A^\dagger A}}. \tag{4.18}$$

We see that in the above relation the calculation of the (inverse) square root of an operator is necessary. The square root of a positive definite non-singular operator can be calculated in different ways. One of the simplest ways (for small matrices) is using the spectral representation.

The spectral representation of an operator is defined by its eigenvalues and eigenvectors. If we assume that we have an operator B with its eigenvalues λ^i and eigenvectors v^i then the spectral representation of this operator is defined by:

$$B_{x,y} \quad = \quad \sum_i \lambda^i v_x^i v_y^{i*}. \tag{4.19}$$

For any function of this operator we can write

$$f(B) \quad = \quad \sum_i f(\lambda^i) v_x^i v_y^{i*}. \tag{4.20}$$

And for the square root of this operator we can then write

$$\sqrt{B}_{x,y} \quad = \quad \sum_i \sqrt{\lambda^i} v_x^i v_y^{i*}. \tag{4.21}$$

So this relation can be used to calculate for positive operators the projection to U(3). The reason for changing the projection from SU(3) to U(3) is that most of the dynamical algorithms are based on molecular dynamics and therefore the differentiation of the action with respect to the gauge fields is needed. Here this is obtained by changing the projection from SU(3) to U(3) [30].

4.6 STOUT Smearing

An important component of any smearing algorithm is the projection back into SU(3). Such a projection is not unique. Therefore it should be defined such that all symmetry properties of the link variables are preserved. We have a given 3×3 Matrix V. We want to project this matrix into SU(3). There are many ways to do this. One way is to do this by an iterative process. The details of some projection methods have been mentioned in the previous section.

There are some problems with projections because of the non-differentiability which is necessary for the Hybrid Monte Carlo algorithm, which requires knowing the response of the action to a small change of the link variables. STOUT smearing is a method which

is analytic everywhere in the finite complex plane and uses an exponential function to stay in SU(3) [22, 31]. Let us look concretely at the STOUT smearing method and how it is defined.

Like in APE smearing we start with a weighted sum of perpendicular staples

$$\begin{aligned} C_\mu(n) &= \sum_{\nu\neq\mu} \rho_{\mu\nu}(U_\nu(n)U_\mu(n+\hat{\nu})U_\nu^\dagger(n+\hat{\mu}) \\ &+ U_\nu^\dagger(n-\hat{\nu})U_\mu(n-\hat{\nu})U_\nu(n-\hat{\nu}+\hat{\mu})), \end{aligned} \tag{4.22}$$

where $\rho_{\mu\nu}$ are adjustable real parameters.
The next definition uses the weighted sum of the perpendicular staples

$$\tilde{\Omega}_\mu(n) = C_\mu(n)U_\mu^\dagger(n). \tag{4.23}$$

One can now go on and use $\tilde{\Omega}_\mu(n)$ to define a matrix $Q_\mu(n)$

$$Q_\mu(n) = \frac{i}{2}\left(\tilde{\Omega}_\mu^\dagger(n) - \tilde{\Omega}_\mu(n)\right) - \frac{i}{2N}\mathrm{tr}\left(\tilde{\Omega}_\mu^\dagger(n) - \tilde{\Omega}_\mu(n)\right). \tag{4.24}$$

$Q_\mu(n)$ is a hermitian traceless matrix and is an element of the algebra of SU(3). From this follows that $\exp(iQ_\mu(n))$ is an element of SU(3). This fact is used to define an iterative analytic link smearing algorithm in which $U_\mu^j(n)$ is mapped on $U_\mu^{j+1}(n)$ using

$$U_\mu^{j+1}(n) = \exp(iQ_\mu^j(x))U_\mu^j(n). \tag{4.25}$$

The point that $\exp(iQ_\mu(n))$ is an element of SU(3) implies that also $U_\mu^{j+1}(n)$ is an element of SU(3). The only open points in the implementation of STOUT smearing are the weights $\rho_{\mu\nu}$. These parameters can be selected in different ways. One can choose them as

$$\rho_{ik} = \rho \quad , \quad \rho_{4\mu} = \rho_{\mu 4} = 0. \tag{4.26}$$

This kind of selection corresponds to a 3-dimensional scheme, where only the spatial links are smeared. This may be useful for constructing hadronic interpolators. Another choice is to select

$$\rho_{\mu\nu} = \rho. \tag{4.27}$$

This is the isotropic four-dimensional scheme.
STOUT smeared link variables have the same symmetry transformation properties as the original link variables. They transform under a local gauge transformation like the original link variables

$$Q_\mu(n) \rightarrow Q'_\mu(n) = \Omega(n)Q_\mu(n)\Omega(n)^\dagger, \tag{4.28}$$

$$e^{iQ_\mu(n)} \rightarrow e^{iQ'_\mu(n)} = \Omega(n)e^{iQ_\mu(n)}\Omega(n)^\dagger, \tag{4.29}$$

$$U_\mu^{(1)}(n) \to U_\mu^{(1)'}(n) = \Omega(n)e^{iQ_\mu(n)}\Omega(n)^\dagger\Omega(n)U_\mu(n)\Omega(n+\hat{\mu})^\dagger = \Omega(n)U_\mu^{(1)}(n)\Omega(n+\hat{\mu})^\dagger \quad (4.30)$$

and also their transformation properties under all rotations and reflections in a plane containing the link are the same as the original link variables [22].

For our further investigations we use an isotropic four dimensional STOUT smearing scheme. Similar arguments like in the case of APE smearing parameter are valid for the STOUT smearing parameter ρ. The plaquette increases for small values of ρ and reaches a maximum around $\rho = 0.2$. So the best value for the parameter is $\rho = 0.1$ [37]. We set our parameter to this value.

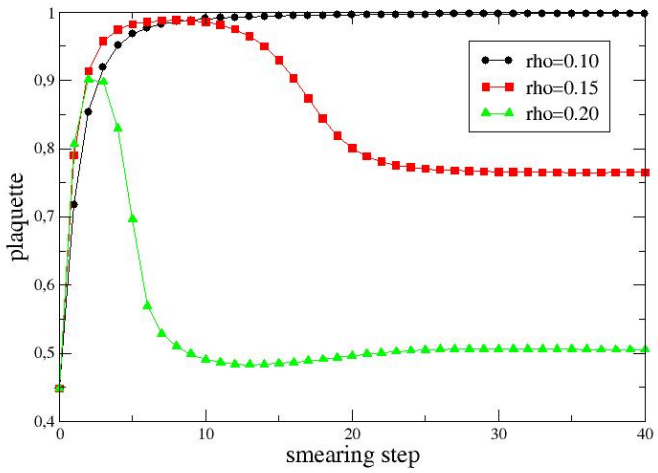

Figure 4.2: Plaquette calculated on a configuration on a $12^3 \times 24$ lattice with $\beta = 4.7$ as a function of the smearing steps for different STOUT smearing parameters.

4.7 Smearing and Static Quark Potential

To illustrate the idea of smearing clearly we study the effect of the smearing on the static quark potential. The technical details how to calculate the static quark potential were discussed in Chapter 3.2.2. The static quark potential is sensitive to the smearing of gauge links. As mentioned smearing suppresses the short distance fluctuations of the gauge configurations. In the language of the static quark potential this means that increased levels of the smearing affect more and more the Coulomb part of the static quark potential [26].

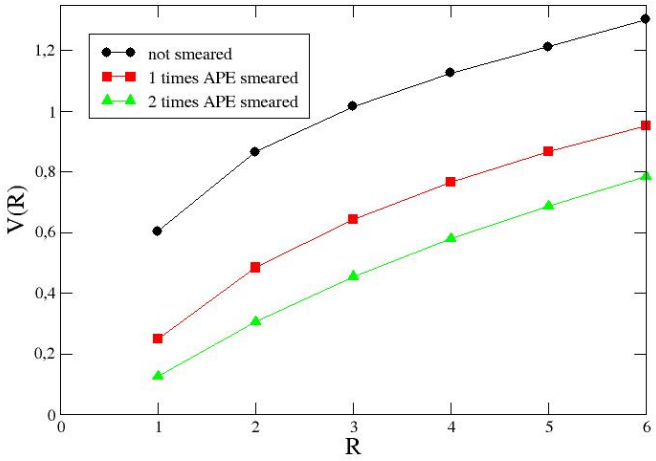

Figure 4.3: Static quark potential for SU(3) as a function of distance R on one times and two times APE smeared configurations. 302 configurations on a $12^3 \times 24$ lattice are used. The coupling parameter is $\beta = 5.3$.

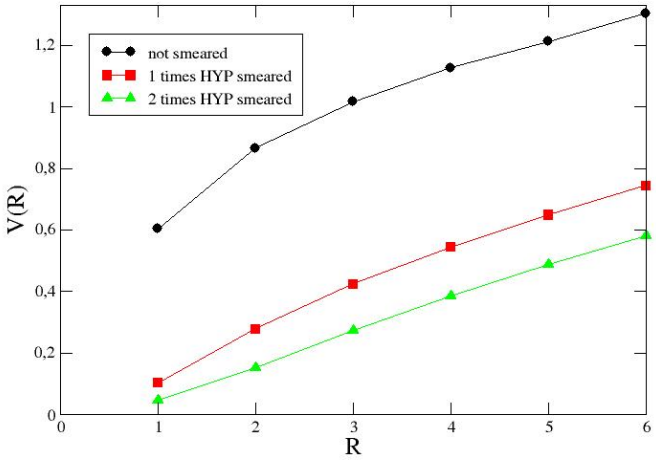

Figure 4.4: Static quark potential for SU(3) as a function of distance R on one times and two times HYP smeared configurations. All the other parameters stay equal as in Fig. 4.3.

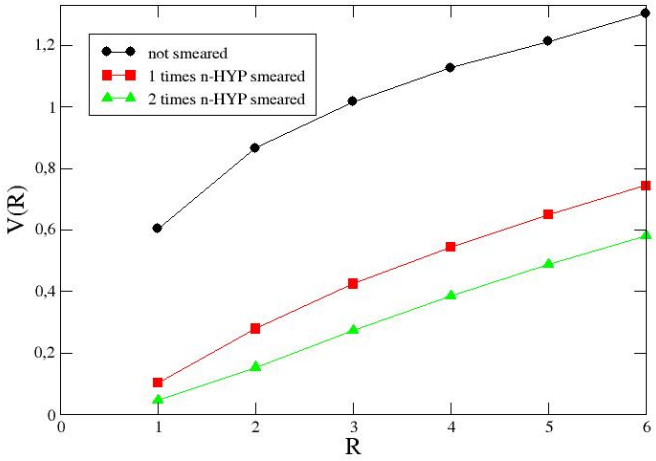

Figure 4.5: Static quark potential for SU(3) as a function of distance R on one times and two times n-HYP smeared configurations. All the other parameters stay equal as in Fig. 4.3.

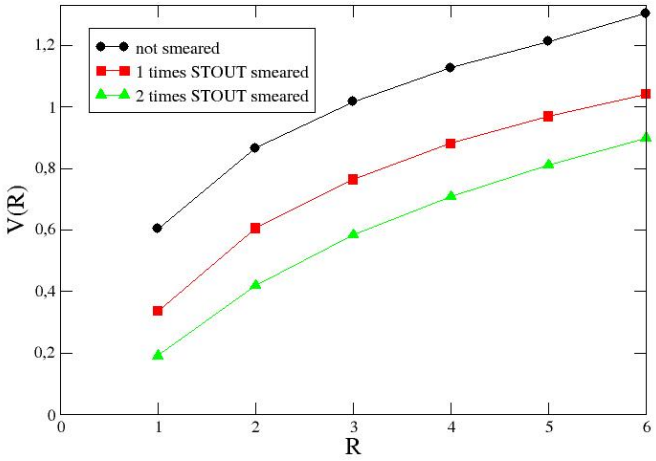

Figure 4.6: Static quark potential for SU(3) as a function of distance R on one times and two times STOUT smeared configurations. All the other parameters stay equal as in Fig. 4.3.

In these figures we see the effect of the smearing on the static quark potential. One can also see that the long distance behavior is unchanged (up to an irrelevant additive constant) because the string tension stays equal. The mentioned effect of smearing on Coulomb part of potential can be computed perturbatively and the obtained deviation from the Coulomb potential is used to introduce a fourth fit parameter in the potential fit. Subtracting this perturbation part gives the correct data. So the effect of the smearing on short distance potential is under good perturbative control [38, 39]. Then one can give the smooth curve in the standard parametrization [40]:

$$V(r) = B - \frac{A}{r} + \sigma r + C\left(\left[\frac{1}{\mathrm{r}}\right] - \frac{1}{r}\right) \tag{4.31}$$

with A, B, C and σ the constants. The perturbative lattice Coulomb potential [1/r] is a correction to continuum Coulomb potential. Also it is worth mentioning that all of these smearing methods have very similar effect on the static quark potential. From these figures we can not make a classification of the smearing methods. We will do these in the next chapters. In the next chapter we will introduce the definition of some local observables for our analysis of the smearing methods.

5 THE CALCULATION OF SOME LOCAL OBSERVABLES

5.1 Motivation

We want to test the effectiveness of some smearing methods. Therefore we need observables which are economic. We now want go through some local observables and discuss how they are defined and how to calculate them.

5.2 The Plaquette

For the gluon action it is sufficient to take the shortest, non-trivial closed loop on the lattice. This loop is the 1×1 Wilson loop, the so-called plaquette. This loop is used to calculate the non-improved gauge action, also called Wilson action. The plaquette is a product of link variables which is defined as

$$\begin{aligned} U_{\mu\nu}(n) &= U_\mu(n)U_\nu(n+\hat{\mu})U_{-\mu}(n+\hat{\mu}+\hat{\nu})U_{-\nu}(n+\hat{\nu}) \\ &= U_\mu(n)U_\nu(n+\hat{\mu})U_\mu(n+\hat{\nu})^\dagger U_\nu(n)^\dagger. \end{aligned} \tag{5.1}$$

One can get a gauge invariant quantity of link variables if one takes ordered products of link variables along a closed loop and then the trace of this loop. We see that the plaquette is the easiest closed loop of such class of loops. So now to get a gauge invariant quantity, we have to take the trace of the plaquette.

If we have a lattice with n sites in 4 dimensions then there are $6n$ site plaquettes. To get the average plaquette we have to add all plaquettes and then to divide this number by the total plaquette number. In addition to normalize this number to maximum value 1 we have to divide by 3, because our gauge link variables are SU(3) elements

$$P_{av} = \frac{1}{3 \cdot 6 \cdot \text{nsite}} \sum_n \sum_{\mu<\nu} \text{ReTr}\left[U_{\mu\nu}(n)\right].$$

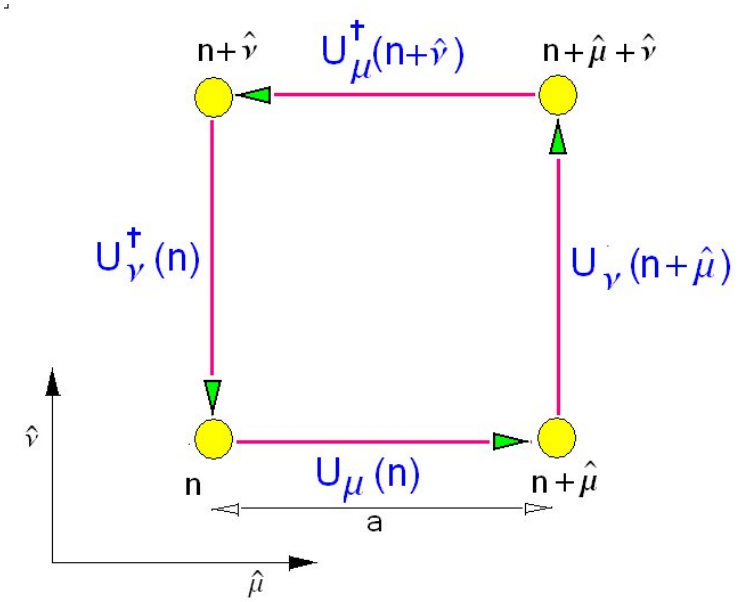

Figure 5.1: 1×1 planar Wilson-loop or the so-called plaquette in the $\mu\nu$-plane based at n. The variable a denote the lattice spacing.

5.3 Rectangular Loop

The next simplest loop after the plaquette is the rectangular Wilson-loop. Such loops are used in order to improve the Wilson gauge action (Lüscher-Weisz gauge action) and to reduce the finite lattice spacing artifacts to an order of a^2 in lattice perturbation theory.

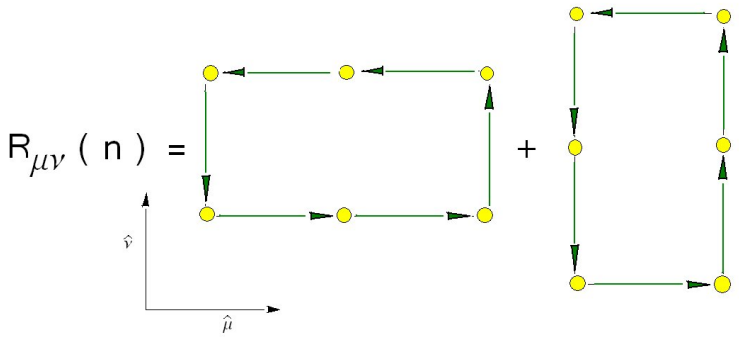

Figure 5.2: The rectangular planar 1×2 and 2×1 loops in $\mu\nu$-plane.

The expression of Fig. 5.2 can be written in terms of the link variables as

$$\begin{aligned} R_{\mu\nu}(n) &= U_\mu(n)U_\mu(n+\hat{\mu})U_\nu(n+2\hat{\mu})U_\mu^\dagger(n+\hat{\mu}+\hat{\nu})U_\mu^\dagger(n+\hat{\nu})U_\nu^\dagger(n) \\ &+ U_\mu(n)U_\nu(n+\hat{\mu})U_\nu(n+\hat{\mu}+\hat{\nu})U_\mu^\dagger(n+2\hat{\nu})U_\nu^\dagger(n+\hat{\nu})U_\nu^\dagger(n). \end{aligned} \tag{5.2}$$

The last step is to take the trace of the rectangular loop to have a gauge invariant object. At each lattice site there are 12 rectangular loops on a four dimensional lattice. Additionally we have to normalize the average rectangle loop through dividing by 3 because of the trace operation of an SU(3) object. Finally we get

$$R_{ave} = \frac{1}{3 \cdot 12 \cdot \text{nsite}} \sum_x \sum_{\mu<\nu} \text{ReTr}\left(R_{\mu\nu}(n)\right). \tag{5.3}$$

5.4 Bent Loop

The bent loop is beside plaquette and rectangles loop another elementary loop on the lattice. This loop also occurs in the improved Lüscher-Weisz gauge action. Another important detail about the bent loop is that it has an extension in 3 dimensions. Let us look at the definition of such a bent loop.

$$B_{\mu\nu\tau}(n) = U_\mu(n)U_\nu(n+\hat{\mu})U_\tau(n+\hat{\mu}+\hat{\nu})U_\nu^\dagger(n+\hat{\mu}+\hat{\tau})U_\mu^\dagger(n+\hat{\tau})U_\tau^\dagger(n). \tag{5.4}$$

The graphical representation of this bent loop is:

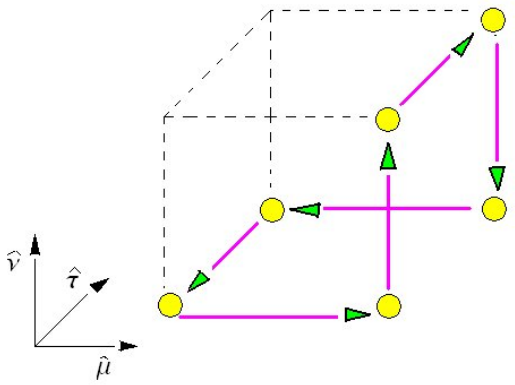

Figure 5.3: One of the bent loops in a cube

In the next step we want to know how many such different bent loops are in a four dimensional lattice. Each bent loop is characterized by a bending edge. Since the bent loop is defined on a cube and since a cube has 12 edges we get alltogether 12 bent loops in a cube. In a d dimensional hypercube there are

$$\binom{d}{3} \tag{5.5}$$

cubes. This would correspond to 4 cubes in 4 dimensions. So we get for a four dimensional hypercube 48 bent loops. In a four dimensional lattice with n sites there are $48n$ bent loops. Like in the case of the average plaquette, we are now able to calculate the average bent loop.

5.5 Twisted Bent Loop

Another example of the elementary Wilson loops which are non planar is the twisted bent or twisted chair loop. Twisted bent loops are used in the tadpole improved Lüscher-Weisz gauge action [41], which is defined as

$$S_g = -\beta_1 \sum_{pl} \frac{1}{3}\mathrm{ReTr}U_{pl} - \beta_2 \sum_{re} \frac{1}{3}\mathrm{ReTr}U_{re} - \beta_3 \sum_{tb} \frac{1}{3}\mathrm{ReTr}U_{tb}. \tag{5.6}$$

In the third term the twisted bent loop contribution to the improved gauge action is visible. Let us look at the definition of the twisted bent loops and its graphical representations. The twisted bent is also defined like the bent loop on an cube because of 3 directions.

$$T_{\mu\nu\tau}(n) = U_\mu(n)U_\nu(n+\hat{\mu})U_\tau(n+\hat{\mu}+\hat{\nu})U_\mu^\dagger(n+\hat{\nu}+\hat{\tau})U_\nu^\dagger(n+\hat{\tau})U_\tau^\dagger(n). \tag{5.7}$$

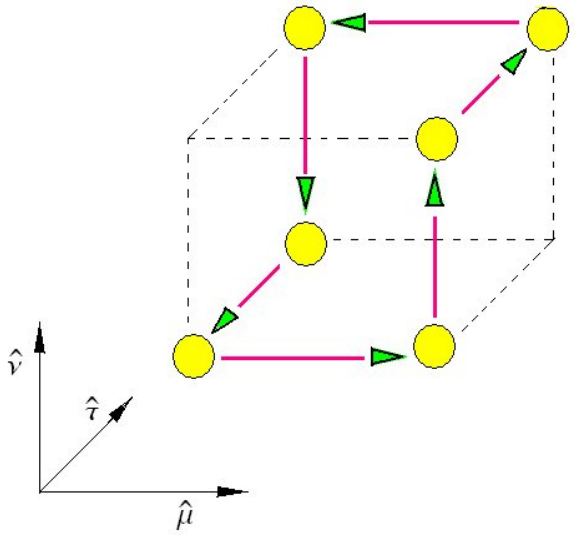

Figure 5.4: A representation of the twisted bent on a cube.

The twisted bent loop is defined like bent loop on a cube. The number of twisted bent loops on a cube corresponds its space diagonals, which is four. A four dimensional hypercube can be seen as 4 cubes. This results in 16 twisted bent loop at each lattice site. In the last step the average twisted bend is calculated like in the case of plaquette by adding of all twisted bent loops and dividing this number by the total loop number and by 3.

5.6 Topological Charge

Topological objects are known to be linked to chiral symmetry breaking and can have a connection to confinement. Therefore the study of topological charge is important. There is no unique definition of the topological charge on the lattice [42]. Filtering methods are necessary to extract a smooth topological density [43, 44]. Fermionic topological charge can be obtained by the use of the eigenmodes of chiral improved Dirac operator [45, 46]. The real modes give the fermionic topological charge. The gluonic topological charge can be obtained by the use of the field tensor. Then one can use smearing methods to extract a smooth topological charge density. The (gluonic) topological charge is a sensitive quantity to smearing methods. It is defined as

$$Q = \frac{1}{32\pi^2}\int d^4x \ \mathrm{tr}\left[\tilde{F}_{\mu\nu}F_{\mu\nu}\right], \tag{5.8}$$

where

$$\tilde{F}_{\mu\nu} = \frac{1}{2}\epsilon_{\mu\nu\rho\sigma}F_{\rho\sigma}. \tag{5.9}$$

This definition can be transferred to the lattice. A possible discretized definition of topological charge is

$$\begin{aligned} Q_L &= \sum_x q_L(x) \\ &= \frac{g^2}{32\pi^2}\epsilon_{\mu\nu\rho\sigma}\sum_x \mathrm{tr}(F_{\mu\nu}(n)F_{\rho\sigma}(n)), \end{aligned} \tag{5.10}$$

where the field strength tensor is

$$a^2 g F_{\mu\nu} = -\frac{i}{8}\left[\left(O^{(1)}_{\mu\nu} - O^{(1)\dagger}_{\mu\nu}\right) - \frac{1}{3}Tr\left(O^{(1)}_{\mu\nu} - O^{(1)\dagger}_{\mu\nu}\right)\right] + O(a^4) \tag{5.11}$$

and $O^{(1)}_{\mu\nu}(x)$ is

$$\begin{aligned} O^{(1)}_{\mu\nu}(n) &= U_\mu(n)U_\nu(n+\mu)U^\dagger_\mu(n+\nu)U^\dagger_\nu(n) \\ &+ U_\nu(n)U^\dagger_\mu(n+\nu-\mu)U^\dagger_\nu(n-\mu)U_\mu(n-\mu) \\ &+ U^\dagger_\mu(n-\mu)U^\dagger_\nu(n-\mu-\nu)U_\mu(n+\mu-\nu)U_\nu(n-\nu) \\ &+ U^\dagger_\nu(n-\nu)U_\mu(n-\nu)U_\nu(n+\mu-\nu)U^\dagger_\mu(n). \end{aligned} \tag{5.12}$$

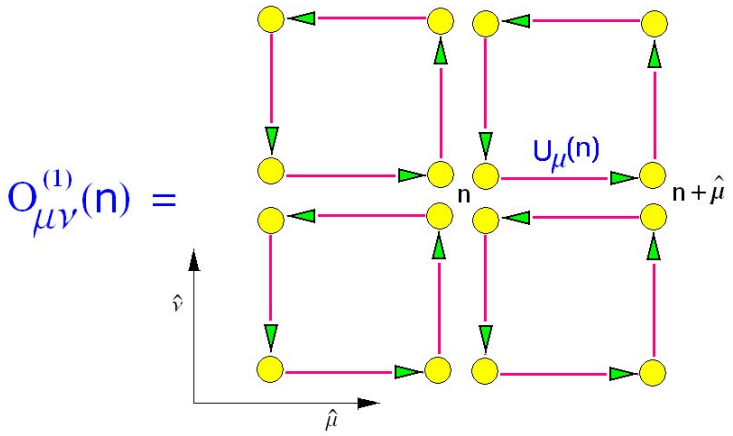

Figure 5.5: Graphical representation of the $O^{(1)}_{\mu\nu}(n)$.

In this form the topological charge operator has large $O(a^2)$ errors, which correspond to an error of 10 percent for a lattice with $\beta = 5.70$ and $a = 0.18$, because even after many smearing steps the topological charge does not take integer values [34]. The way to improve topological charge calculations is to improve the definition of the field tensor. So we take a linear combination of plaquette and rectangular loops [21]

$$O^{(2)}_{\mu\nu}(n) \quad = \quad c_1 O^{(1)}_{\mu\nu}(x) + \frac{c_2}{u_0^2} I^{(2)}_{\mu\nu}(n) \tag{5.13}$$

to reduce $O(a^2)$ errors.

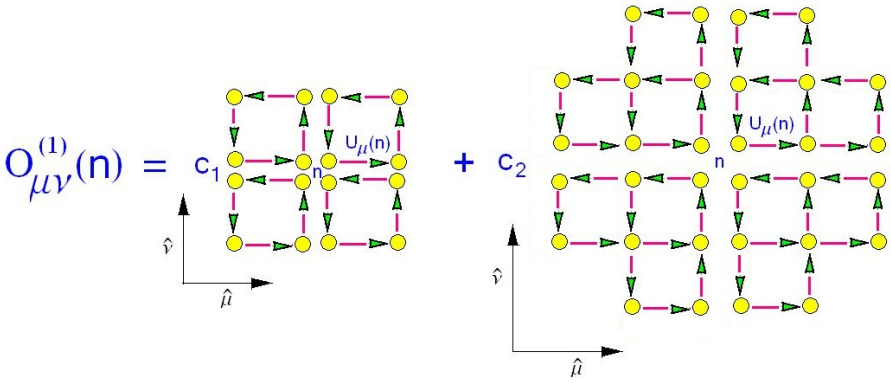

Figure 5.6: Graphical representation of the $O^{(2)}_{\mu\nu}(n)$.

In the above relation the coefficient u_0 is the tadpole coefficient which is defined as

$$u_0 \quad = \quad \left[\frac{1}{3}\mathrm{ReTr}\left(U_\mu(n)U_\nu(n+\hat{\mu})U_\mu(n+\hat{\nu})^\dagger U_\nu(n)^\dagger\right)\right]^{1/4} \tag{5.14}$$

and the coefficients for an $O(a^2)$ improved $F_{\mu\nu}$ are

$$c_1 = \frac{5}{3} \quad \text{and} \quad c_2 = -\frac{1}{6}. \tag{5.15}$$

$I^{(2)}_{\mu\nu}(n)$ is the link products of 1×2 and 2×1 rectangles in $\mu\nu$-plane. It is defined by

$$\begin{aligned}
I^{(2)}_{\mu\nu}(n) &= U_\mu(n)U_\mu(n+\hat{\mu})U_\nu(n+2\hat{\mu})U^\dagger_\mu(n+\hat{\mu}+\hat{\nu})U^\dagger_\mu(n+\hat{\nu})U^\dagger_\nu(n) \\
&+ U_\mu(n)U_\nu(n+\hat{\mu})U_\nu(n+\hat{\mu}+\hat{\nu})U^\dagger_\mu(n+2\hat{\nu})U^\dagger_\nu(n+\hat{\nu})U^\dagger_\nu(n) \\
&+ U_\nu(n)U_\nu(n+\hat{\nu})U^\dagger_\mu(n-\hat{\mu}+2\hat{\nu})U^\dagger_\nu(n-\hat{\mu}+\hat{\nu})U^\dagger_\nu(n-\hat{\mu})U_\nu(n-\hat{\mu}) \\
&+ U_\nu(n)U^\dagger_\mu(n-\hat{\mu}+\hat{\nu})U^\dagger_\mu(n-2\hat{\mu}+\hat{\nu})U^\dagger_\nu(n-2\hat{\mu})U_\mu(n-2\hat{\mu})U_\mu(n-\hat{\mu}) \\
&+ U^\dagger_\mu(n-\hat{\mu})U^\dagger_\mu(n-2\hat{\mu})U^\dagger_\nu(n-2\hat{\mu}-\hat{\nu})U_\mu(n-2\hat{\mu}-\hat{\nu})U_\mu(n-\hat{\mu}-\hat{\nu})U_\nu(n-\hat{\nu}) \\
&+ U^\dagger_\mu(n-\hat{\mu})U^\dagger_\nu(n-\hat{\mu}-\hat{\nu})U^\dagger_\nu(n-\hat{\mu}-2\hat{\nu})U_\mu(n-\hat{\mu}-2\hat{\nu})U_\nu(n-2\hat{\nu})U_\nu(n-\hat{\nu}) \\
&+ U^\dagger_\nu(n-\hat{\nu})U_\mu(n-\hat{\nu})U_\mu(n+\hat{\mu}-\hat{\nu})U_\nu(n+2\hat{\mu}-\hat{\nu})U^\dagger_\mu(n+\hat{\mu})U^\dagger_\mu(n) \\
&+ U^\dagger_\nu(n-\hat{\nu})U^\dagger_\nu(n-2\hat{\nu})U_\mu(n-2\hat{\nu})U_\nu(n+\hat{\mu}-2\hat{\nu})U_\nu(n+\hat{\mu}-\hat{\nu})U^\dagger_\mu(n).
\end{aligned} \tag{5.16}$$

The graphical representation of such a combination is given in Fig. 5.6.

Here we can make a test of our definition of the topological charge. It should take integer values as a function of the smearing method

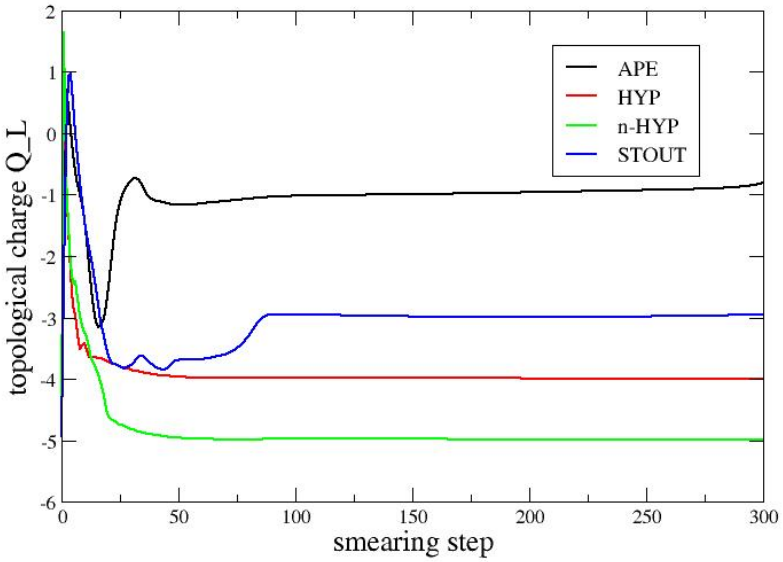

Figure 5.7: Topological charge calculated on a $16^3 \times 24$ configuration as a function of smearing step for different smearing methods.

From this figure we see that this definition satisfy the condition. For APE smearing topological charge takes around 60, for HYP and n-HYP around 40 and for STOUT around 80 smearing steps integer values

After we have studied the definition of some local observables on the lattice, we are going to use this expressions in our analysis of some smearing methods, which were defined in the Chapter 3.

6 SMEARING METHODS AS MONTE CARLO RENORMALIZATION GROUP TRANSFORMATIONS

6.1 Introduction

Monte Carlo methods can be used to study the critical properties of systems. This is done by the determination of long distance properties through calculation of the extended observables, like correlation functions. This way is connected to problems like boundary and fine size effects, which makes the extrapolation from finite to infinite systems so difficult. The reason for this problems is that the correlation length diverges as the critical temperature is approached, but it is found to be finite on finite lattices [47, 48, 49]. Various singularities of interest at a critical point are rounded off in the finite systems, preventing us from taking "useful" data extremely close to the $T \to T_c$.

It is also possible to use a combination of renormalization group(RG) and Monte Carlo methods referred to as Monte Carlo renormalization group or real space renormalization group transformations to study the critical properties of the systems [47, 50]. In the Monte Carlo renormalization method one studies the renormalization properties of the system with regard to local observables defined on small length scales. This method is very useful to get reliable results. Originally it was used for spin systems [48, 51, 52].

6.2 Monte Carlo Renormalization Group Transformations

The main idea of Monte Carlo renormalization group transformations is to simplify the calculations in a system in a way that does not affect the critical properties of a system and to focus attention on the critical properties of interest in the system as well. In other words renormalization group transformations do not change long distance behavior of a system [47, 48].

As mentioned it is possible to combine renormalization group and Monte Carlo methods. In a Monte Carlo simulation a sequence of configurations is generated. The details of this generation have been discussed in previous Chapter 3. The lattice action for a pure Yang-Mills theory which corresponds to these configurations can in general be written as

$$-S[U] = \sum_{\alpha} \beta_\alpha S_\alpha[U], \tag{6.1}$$

where $\{S_\alpha[U]\}$ are traces of Wilson loops (or products thereof) and $\{\beta_\alpha\}$ are the corresponding coupling constants.

In the next step the idea of block-spin transformations for spin systems is used. In block-spin transformations spin variables on neighboring sites are grouped in blocks and averaged to a block-value. This procedure is in some way integrating out the short-wavelength fluctuations while affecting the long-wavelength correlations as little as possible. The size of the system is reduced by a factor b. The number of spins in a block is b^d, where d is the dimension of the system [48].

So one use the renormalization group transformations in real space in the same sense as block-spin transformations. The repeated renormalization group transformations or block spin transformations correspond to a path in an infinite dimensional space of coupling constants.

If the original theory is scale invariant, then the block spin transformation will leave the theory scale invariant. Near the phase transition the correlation length ξ diverges. This defines a subspace of the infinite dimensional space of coupling constants, called critical surface with the property $\xi = \infty$.

At this point the concept of the fixed points appears in our consideration. Once if one is in the critical surface, then the repeated application of the block spin transformations will lead towards a particular point, the so-called fixed point. A fixed point is invariant under block spin transformations. If one starts near the critical surface($\xi \neq \infty$), then the block spin transformations would decrease the correlation length to ξ/b, so that the trajectory moves away from the critical surface [53].

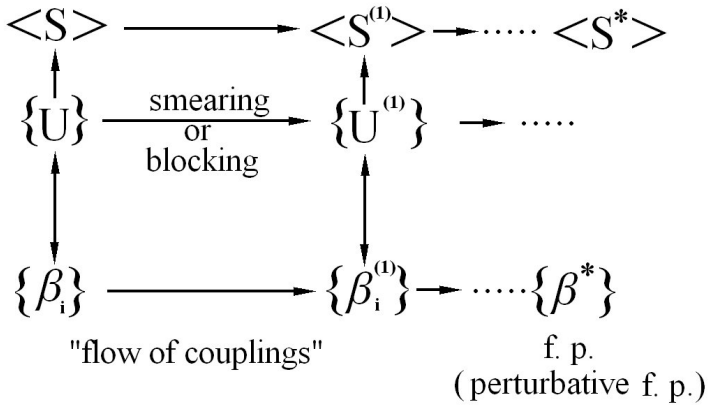

Figure 6.1: Sketch of flow of ensembles, coupling constants and operators to the fixed point.

6.3 Smearing Methods as Block Spin Transformations

6.3.1 Flow of the Observables

One can (at least, in principle) calculate the lattice action for a pure Yang-Mills theory, which corresponds to the set of blocked configurations.

$$-S[U'] = \sum_{\alpha} \beta'_{\alpha} S_{\alpha}[U']. \tag{6.2}$$

The blocked action calculated on these configurations differs from the action of the initial configurations having different coupling constants $\beta_j^{'}$. By repeating the block spin transformations one obtains a fixed point β^* behavior of the blocked action. That means

$$\beta^{'}(\beta^*) = \beta^*. \tag{6.3}$$

If the fixed point action contains local interaction terms then one can study fixed point properties on local observables. We want to proceed in the following way. Assume we have a configuration. From the link variables of this configuration the block links are obtained through smearing procedures. Smearing methods which are taken into account in this consideration are APE-smearing, HYP-smearing, n-HYP-smearing and STOUT-smearing. The details of this smearing methods were studied in Chapter 4. In the case of smearing considered as block spin transformations is the scale factor $b = 1$. Now we want to study the flow of the observables and then the flow of the renormalized couplings under these block spin transformations. The observables which are considered are:

(1)... Plaquette

(2)... Rectangular Loop

(3)... Bent Loop

(4)... Twisted Bent Loop

(5)... Topological Charge

The first four of these observables are local and therefore good candidates to study the effect of these block spin transformations, which are in this case different smearing methods. The topological charge is defined globally and its behavior under smearing is of physical interest. The technical details for the calculation of these observables have been discussed in Chapter 5. The configurations which we use here are Hybrid Monte Carlo generated for $n_f = 2$ mass degenerate quarks with a chirally improved Dirac operator [45, 46] and the improved Lüscher-Weisz gauge action [41].

The parameters of the configurations which are used in this analysis are:

$L^3 \times T$	β_1	am	$a[fm]$	config.
$16^3 \times 32$	4.58	0.077	0.1414	302

Table 6.1: The parameters for the generation of configurations. $L^3 \times T$ denotes the extend of the lattice in units of lattice spacing a. β_1 is the dominant coupling from the three Lüscher-Weisz gauge action couplings. 302 configurations have been generated separated by 5 HMC-trajectories [40].

As mentioned the repeated application of a block spin transformation leads to a fixed point. This characteristic is also satisfied for the smearing methods. One can observe this in the calculation of the above cited local observables on the often smeared configurations.

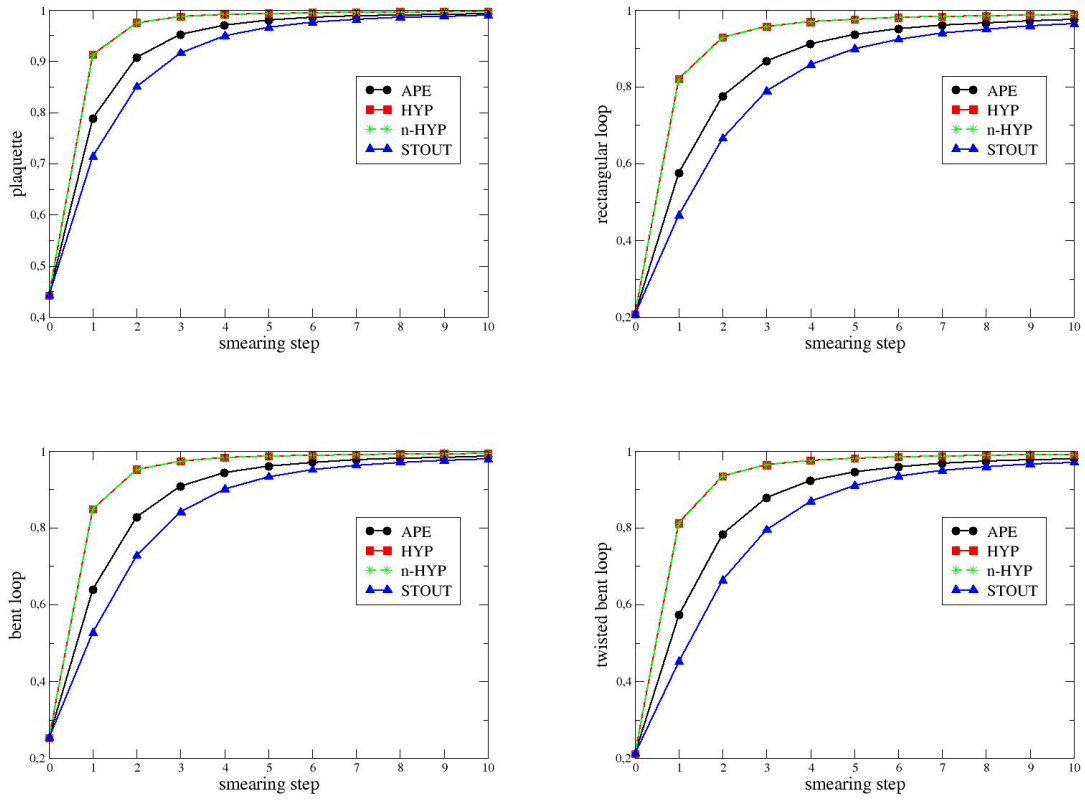

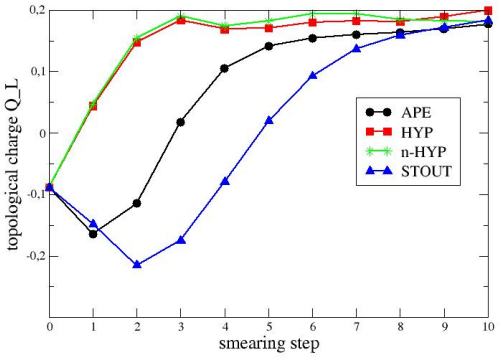

Figure 6.2: Calculation of the observables plaquette, rectangular loop, bent loop, twisted bent loop and topological charge on repeatedly blocked lattices. The blocking steps corresponds to the smearing steps. The lattice size is 16^3x32. The smear parameters which we use for various smearing methods are: $\alpha = 0.55$ (APE), $\alpha_1 = 0.75, \alpha_2 = 0.6, \alpha_3 = 0.3$ (HYP), $\alpha_1 = 0.75, \alpha_2 = 0.6, \alpha_3 = 0.3$ (n-HYP), $\rho = 0.10$ (STOUT).

From these figures one can see a comparison of different smearing methods. These show how various smearing methods differ and in some sense the running behavior towards the fixed point. Another important aspect of these figures is to show the effect of the repeated performing of the different renormalization group transformations for the same observable. So these figures make clear the different behavior of the observables which we use under the different smearing methods. For example, the flow of the topological charge is not so fast as the flow of the the other observables. A better observable than the topological charge is the topological charge susceptibility defined as

$$\chi_t = \langle Q_L^2 \rangle - \langle Q_L \rangle^2 . \tag{6.4}$$

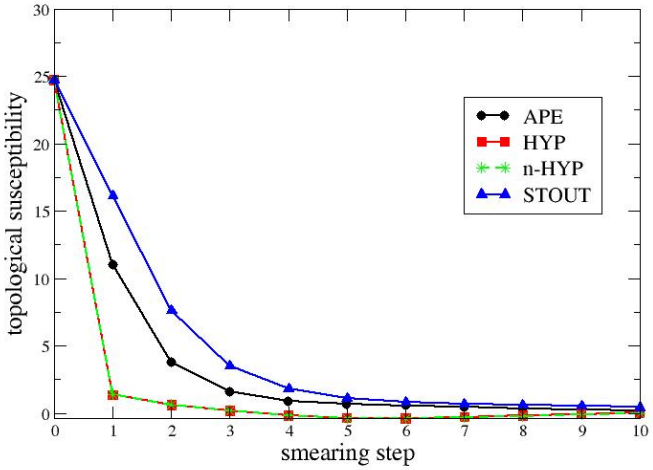

Figure 6.3: Calculation of the observable topological charge susceptibility on repeated smeared lattices. All the parameters referred to different smearing methods stay equal as in Fig. 6.2.

The topological susceptibility shows a good flow behavior towards zero. Another important aspect is that the running behavior of the effect of each smearing method stays equal like in the plots above of the other observables.

We can visualize our results in a different way. We plot the n times block configuration observables against another $n+1$ times block configuration observables in different plots for each smearing method. That shows the $n+1$ blocked observable a function of n times blocked observable.

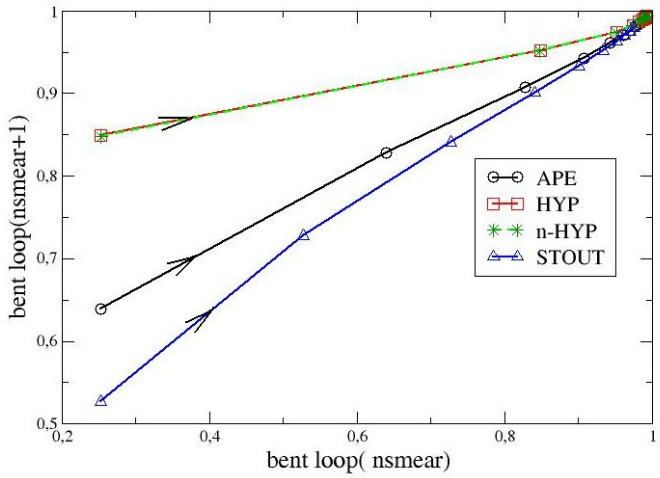

Figure 6.4: Plot of n+1 times smeared observable bent loop versus n times smeared observable bent loop for different smearing methods. All the parameters referring to smearing methods are the same as in Fig. 6.2.

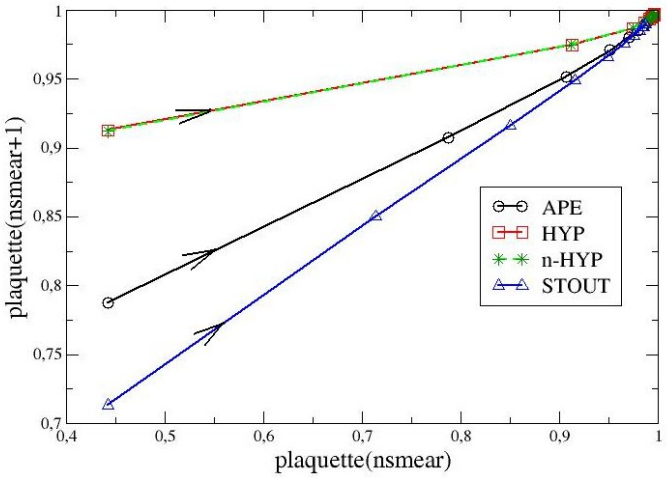

Figure 6.5: Plot of n+1 times smeared observable plaquette versus n times smeared observable plaquette for different smearing methods. All the parameters referring to smearing methods are the same as in Fig. 6.2.

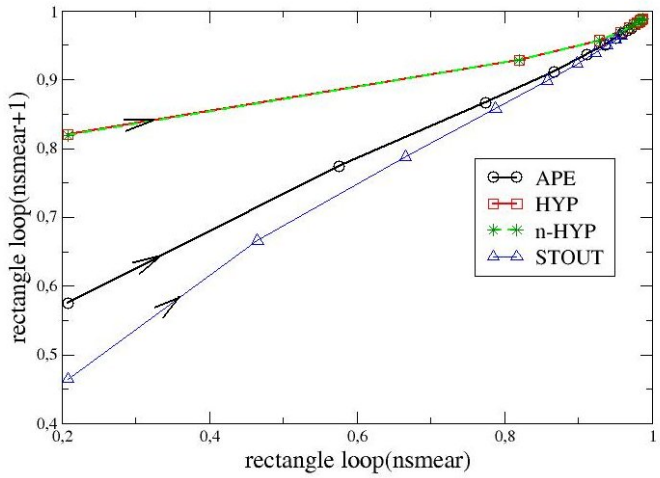

Figure 6.6: Plot of n+1 times smeared observable rectangle loop versus n times smeared observable rectangle loop for different smearing methods. All the parameters referring to smearing methods are as in Fig. 6.2.

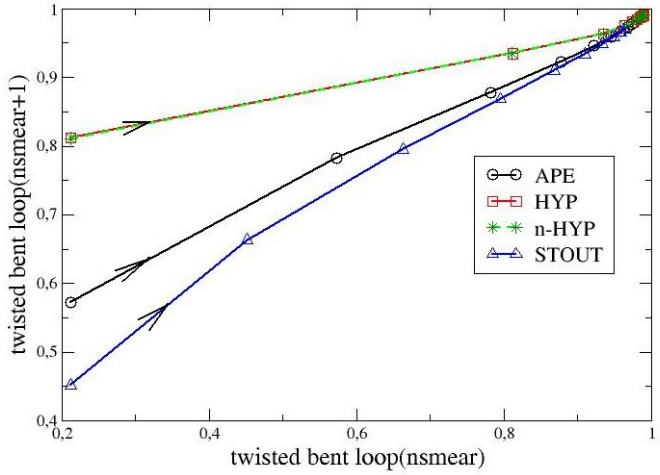

Figure 6.7: Plot of n+1 times smeared observable twisted bent loop versus n times smeared observable twisted bent loop for different smearing methods. All the parameters referring to smearing methods are as in Fig. 6.2.

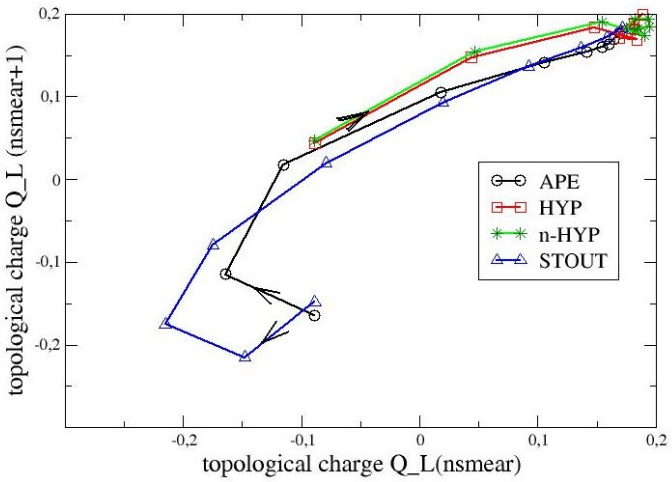

Figure 6.8: Plot of n+1 times smeared observable topological charge Q_L versus n times smeared observable topological charge Q_L for different smearing methods. All the parameters referring to smearing methods are as in Fig. 6.2.

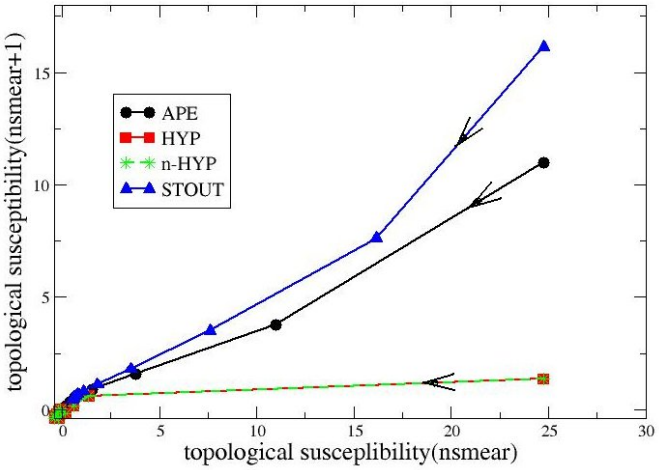

Figure 6.9: Plot of n+1 times smeared observable topological charge susceptibility Q_L versus n times smeared observable topological charge Q_L for different smearing methods. All the parameters referring to smearing methods are as in Fig. 6.2.

At this stage a crude estimate between the effectiveness of different smearing methods can be found by the analysis of the velocity of different smearing methods in the plots above. This estimate can be written as an approximate ratio

$$APE : HYP : STOUT \approx 2 : 1 : 3. \tag{6.5}$$

This ratio means that one HYP smearing roughly corresponds two times APE and three times STOUT. Concerning n-HYP smearing it has nearly the same effectiveness as the HYP smearing.

Let us interpret our results from another perspective. From this aspect the different behavior of various observables under smearing methods can be seen. We plot a n times blocked configuration observable against another n times blocked configuration observable. That would mean the observable O_i is a function of observable O_j. The dependence of one observable on the other can be studied. This way the flow in the space of the observables (analog to the space of couplings) is visualized.

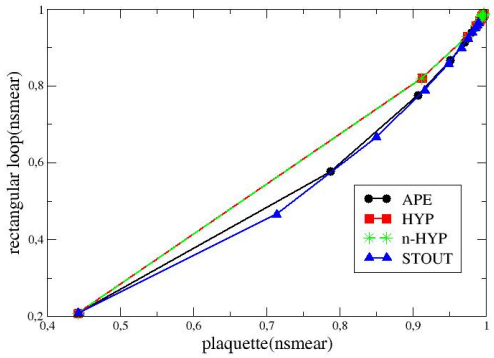

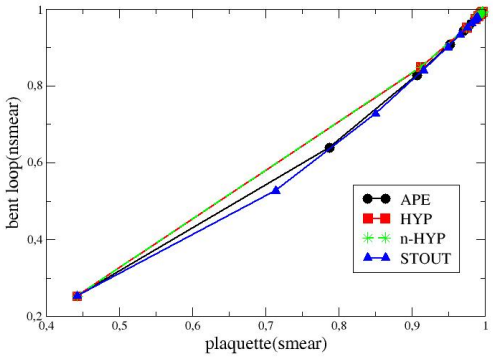

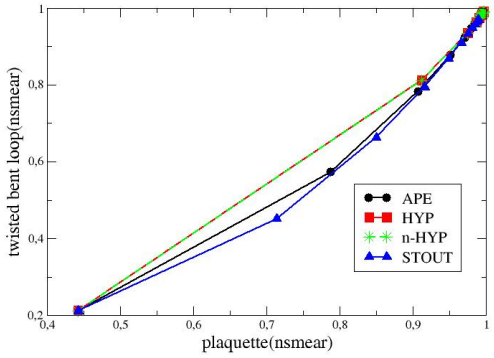

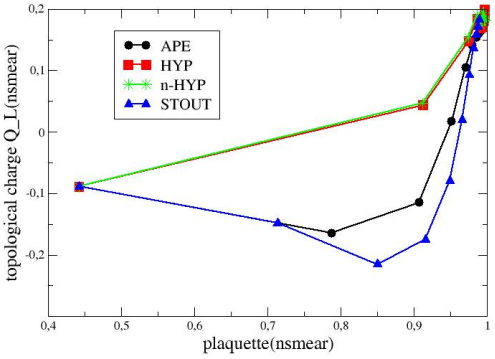

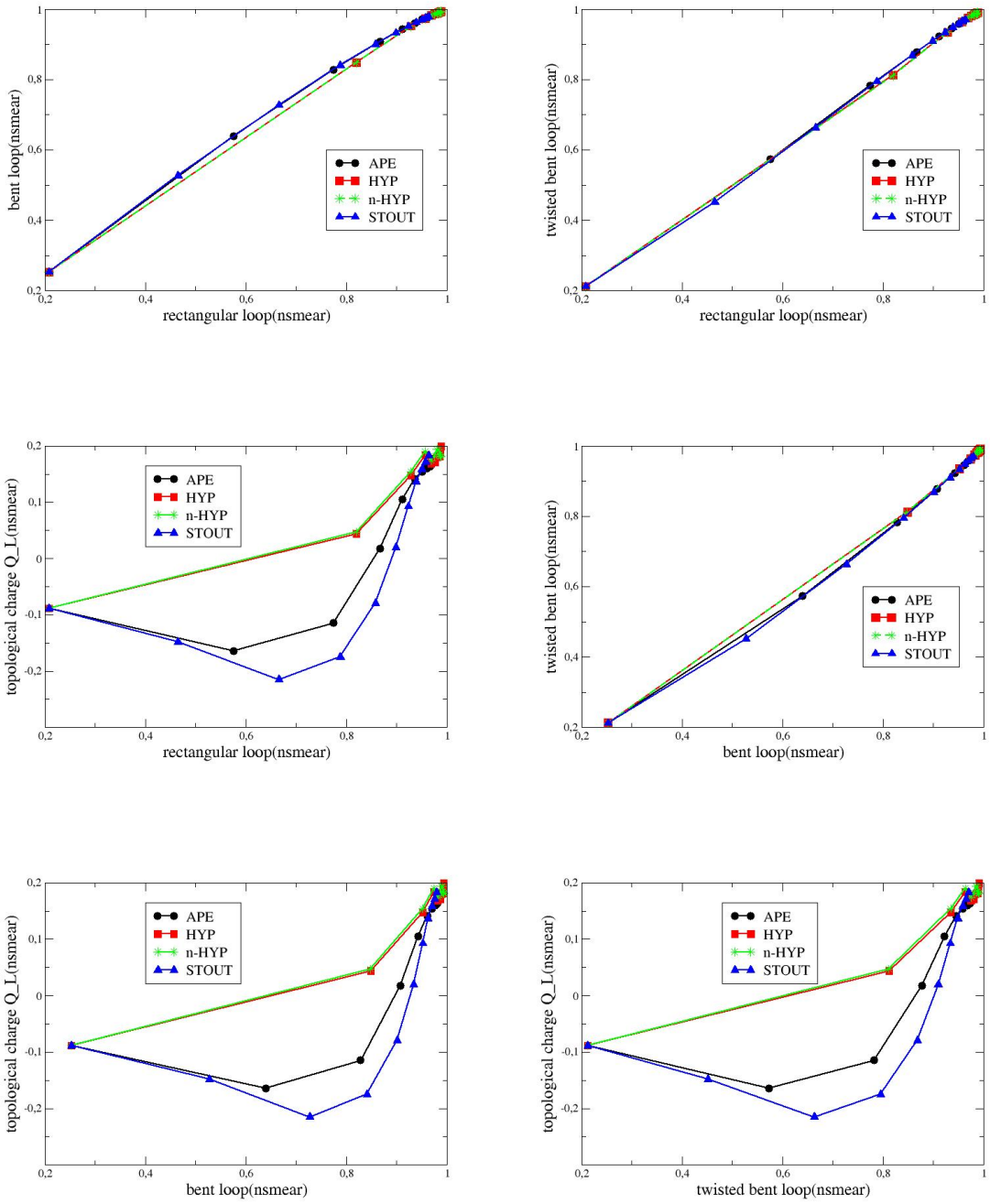

Figure 6.10: Plot of a smeared observable versus another smeared observable.

From these plots in Fig. 6.10 we can extract two important issues for our different smearing methods. The first one concerns the ratio which we gave in (6.5). The second important remark is that the different observables show different flow behavior under the smearing methods. If there would be no difference we would get straight lines in the Fig. 6.10. We see that in plots with rectangular loop, bent loop and twisted bent loop values nearly a straight line is obtained. That corresponds to an almost equal velocity of the flow. In contrast to these observables the plaquette shows a higher flow velocity. The discrepancy of the topological charge is the most obvious. The topological charge show a different behavior as the other observables. Therefore we can again discuss instead of the topological charge the so-called topological susceptibility.

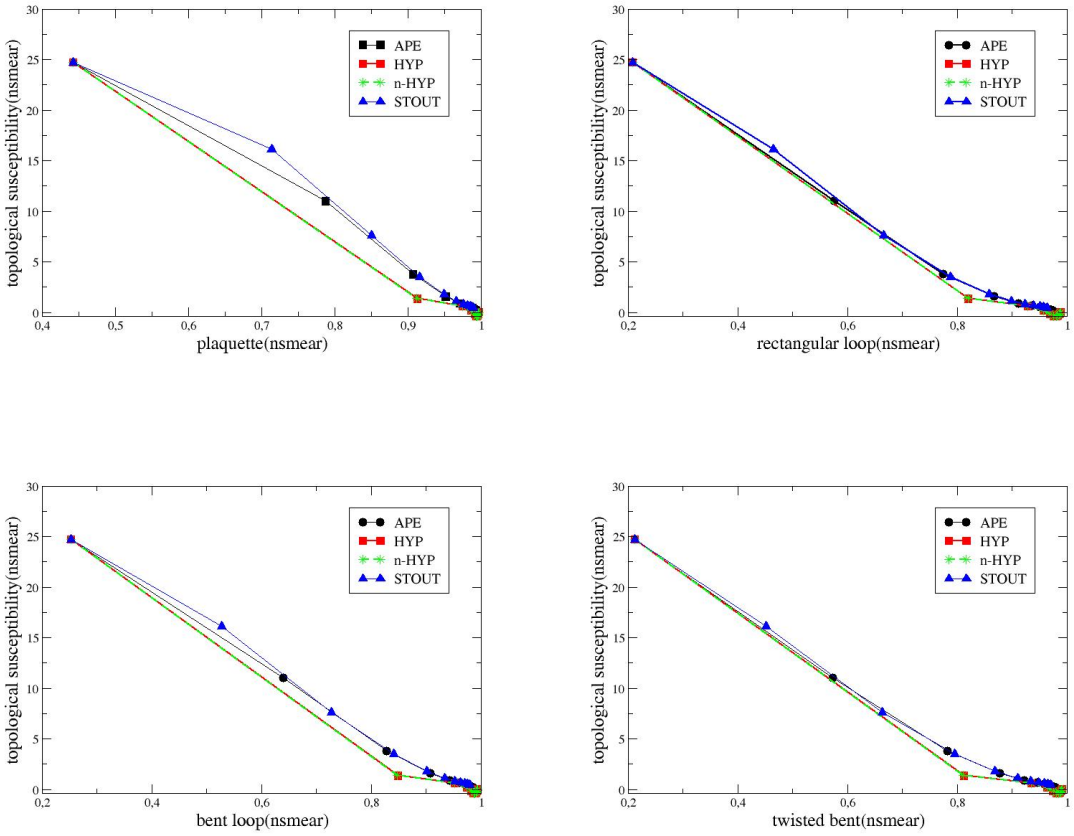

Figure 6.11: Plot of a smeared observable versus another smeared observable.

The topological susceptibility shows in contrast to the topological charge similar flow behavior as the rectangular loop, bent loop and twisted bent loop but the direction of the flow is different.

We now summarize our observations concerning the flow behavior of different observables smearing methods.

(1)... There is a great difference in flow velocity between HYP smearing, APE smearing, STOUT smearing and the difference between HYP and n-HYP smearing is very small.

(2)... One can give a speed ratio estimate.

(3)... All of the observables except the topological charge show a flow behavior towards 1. The topological charge shows a flow behavior towards 0.

(4)... The topological susceptibility is a better observable in our analysis. On the one side it has the properties of the topological charge and on the other side it shows the effect of the smearing better than the topological charge.

6.3.2 Flow of the Coupling Constants

In the Real space renormalization group one has to deal with an infinite number of coupling constants due to the effect of renormalization group transformations. Even if one starts with an ensemble of configurations due to an action with few non-zero couplings, the block spin transformations leads to ensembles with many non-vanishing couplings.

In Monte Carlo renormalization group one can deal with a large number of couplings in contrast to perturbative renormalization group where the number of coupling constants is small. It is possible to increase the number of coupling constants and to estimate the effect [54].

Now we want to study the flow of the coupling constants. Before that it is useful to repeat the classification of the different sort of fixed points. There are three kinds of fixed points. These are trivial fixed points with vanishing correlation length, critical fixed points with infinite correlation length and discontinuity fixed points characteristic for transitions of first order [49]. We want to look for a saturation of the renormalization group flow in the space of couplings. Consequently this flow should lead to the fixed point behavior along a so-called renormalized trajectory.

We assume that the renormalized coupling constants are analytic functions of the original coupling constants $\beta'(\beta)$. Then if we start very near the critical fixed point, the renormalized couplings will initially stay close to the fixed point and move towards the fixed point. However repeating the RG transformation reduces the renormalized correlation length. Consequently the trajectory moves away from the critical fixed point along a so-called renormalized trajectory. The critical exponents are determined by how fast each RG transformation brings the renormalized local observables away from fixed point. At the fixed point β^* with the property $\beta^{'}(\beta^*) = \beta^*$ we can linearize $\beta'(\beta)$ [50, 54]:

$$\beta'_j(\beta) = \beta^*_j + T^*_{jk}(\beta - \beta^*)_k + \mathcal{O}(||\beta - \beta^*||), \tag{6.6}$$

where

$$T_{jk} = \frac{\partial \beta_j}{\partial \beta_k}. \tag{6.7}$$

T^*_{jk} can be obtained from

$$T^{(n+1,n)}_{jk} = \frac{\partial \beta^{(n+1)}_j}{\partial \beta^{(n)}_k} \tag{6.8}$$

at the fixed point

$$T^{(n+1,n)}_{jk} \to T^*_{jk} \quad \text{for} \quad n \to \infty. \tag{6.9}$$

For the calculation of the T-matrix cross-correlations between the observables can be used

$$\frac{\partial \left\langle S^{(n+1)}_i \right\rangle}{\partial \beta^{(n)}_k} = \sum_j \frac{\partial \beta^{(n+1)}_j}{\partial \beta^{(n)}_k} \frac{\partial \left\langle S^{(n+1)}_i \right\rangle}{\partial \beta^{(n+1)}_j}. \tag{6.10}$$

Now we want to show explicitly how such a cross correlator between the operators is calculated. Therefore we start from the action given in (6.1):

$$-S[U] = \sum_\alpha \beta_\alpha S_\alpha[U].$$

The partition function is given by

$$Z = \sum_U e^{-S[U]} = \sum_U e^{\sum_\alpha \beta_\alpha S_\alpha[U]}.$$

The expectation value of an operator i is

$$\langle S_i \rangle = \frac{\partial}{\partial \beta_i} \ln(Z) = \frac{1}{Z} \sum_U S_i[U]\ e^{\sum_\alpha \beta_\alpha S_\alpha[U]}. \tag{6.11}$$

The second derivative is

$$\begin{aligned} \frac{\partial \langle S_i \rangle}{\partial \beta_j} &= \frac{\partial}{\partial \beta_j} \frac{1}{Z} \sum_U S_i[U]\ e^{\sum_\alpha \beta_\alpha S_\alpha[U]} \\ &= \frac{1}{Z} \sum_U S_i[U] S_j[U]\ e^{\sum_\alpha \beta_\alpha S_\alpha[U]} - \frac{1}{Z} \sum_U S_i[U]\ e^{\sum_\alpha \beta_\alpha S_\alpha[U]} \frac{1}{Z} \sum_U S_j[U]\ e^{\sum_\alpha \beta_\alpha S_\alpha[U]} \\ &= \left(\langle S_i S_j \rangle - \langle S_i \rangle \langle S_j \rangle \right). \end{aligned} \tag{6.12}$$

The derivatives in the equation (6.10) can be determined from cross-correlations between operators after n and $n+1$ blocking steps

$$\frac{\partial \left\langle S^{(n+1)}_i \right\rangle}{\partial \beta^{(n)}_k} = \left\langle S^{(n+1)}_i S^{(n)}_k \right\rangle - \left\langle S^{(n+1)}_i \right\rangle \left\langle S^{(n)}_k \right\rangle \equiv B \tag{6.13}$$

and from cross correlations between the operators after $n+1$ blocking steps.

$$\frac{\partial \left\langle S_i^{(n+1)} \right\rangle}{\partial \beta_j^{(n+1)}} = \left\langle S_i^{(n+1)} S_j^{(n+1)} \right\rangle - \left\langle S_i^{(n+1)} \right\rangle \left\langle S_j^{(n+1)} \right\rangle \equiv C \tag{6.14}$$

By considering these equations for a fixed blocking step we can write the equation (6.10) as

$$B = CT. \tag{6.15}$$

Here are B, C, and T quadratic matrices with the size corresponding to the number of the operators (and couplings) used. This is in general a set of linear equations which can be solved for the matrix $T^{(n+1,n)}$

$$T = C^{-1}B. \tag{6.16}$$

For each smearing step n we get such a T-matrix. $T^{(n+1,n)}$ shows the effect of the renormalization group transformations.

The eigenvalues of the matrix $T^{(n+1,n)}$ give estimates for the critical exponents, if one is close to the fixed point. In principle, the matrix $T^{(n+1,n)}$ has an infinite number of components therefore we consider here the truncated form of it. More precisely the matrix $T^{(n+1,n)}$ is constructed on a finite number of operators. So in this method there are two kinds of error sources for the determination of the eigenvalues. These come from truncated matrix $T^{(n+1,n)}$ and from truncation itself. MCRG can be used to find out the effect of including more operators in the calculation. Then the effect of the change resulting from including more operators can be estimated.

For our truncated matrix $T^{(n+1,n)}$ the eigenvalues are determined from the eigenvalue equation

$$T^{(n+1,n)}\phi^i = \lambda^i \phi^i. \tag{6.17}$$

The eigenvalues $\{\lambda\}$ at the fixed point values of the linearized renormalization group transformation gives a classification of the operators(coupling) on the fixed point [54]:

(a) $\lambda > 1$ relevant operator

(b) $\lambda = 1$ marginal operator

(c) $\lambda < 1$ irrelevant operator

The largest eigenvalue has a value which is greater than one. This eigenvalue describes how fast the renormalized operators move away from the fixed point. The largest eigenvalues of $T^{(n+1,n)}$ are used to estimate the critical exponents. The exponents of the

eigenvalue y_T are defined by

$$\lambda = b^{y_T}. \tag{6.18}$$

From this equation it is possible to calculate the critical exponents

$$\nu \equiv \frac{1}{y_T} = \frac{\ln(b)}{\ln(\lambda_i)}. \tag{6.19}$$

This critical exponent describes the divergence of the correlation length as a function of temperature

$$\xi = \frac{1}{|\beta - \beta_c|^{\nu}}. \tag{6.20}$$

In our consideration of smearing methods as BST or MCRG transformations the eigenvalues of T matrix related to the smearing trajectory. The eigenvalues of T characterize and quantify the flow of couplings under the smearing transformations. It starts somewhere and go in direction of the trivial fixed point. We can use this method to calculate the smearing trajectory for different smearing methods and then compare these trajectories to find information about the flow behavior of different smearing methods and also about the effectiveness of different smearing methods. Now we list our eigenvalues of different smearing methods and compare them in the Tables 6.2-6.5.

Blocking Steps	λ_1	λ_2	λ_3	λ_4	λ_5
1	3.8965	1.5976	1.1591	0.7694	0.2682
2	2.5089	1.6564	1.2051	0.9205	0.5451
3	1.9801	1.6098	1.0229	0.8683	0.8115
4	1.6972	1.4688	1.0315	0.9414	0.8855
5	1.5346	1.3467	1.0118	1.0118	0.9185
6	1.4253	1.2715	1.0165	1.0165	0.9440
7	1.3422	1.2206	1.0207	1.0207	0.9616
8	1.2778	1.1783	1.0268	1.0268	0.9734
9	1.2282	1.1423	1.0315	1.0315	0.9800
10	1.1952	1.1151	1.0323	1.0323	0.9838

Table 6.2: Eigenvalues of T-matrix of the APE Smearing.

Blocking Steps	λ_1	λ_2	λ_3	λ_4	λ_5
1	3.9678	1.0084	0.5633	0.1648	0.0636
2	4.4887	2.5397	0.8828	0.8828	0.6963
3	1.9864	1.8587	0.9950	0.9950	0.8945
4	1.6018	1.4186	1.0360	1.0360	0.9477
5	1.3836	1.2382	1.0395	1.0395	0.9669
6	1.2218	1.1611	1.0578	1.0578	0.9719
7	1.1581	1.1581	1.0513	1.0513	0.9775
8	1.1890	1.1332	1.0314	1.0314	0.9841
9	1.1339	1.1143	1.0343	1.0343	0.9887
10	1.1204	1.0694	1.0694	1.0219	0.9932

Table 6.3: Eigenvalues of T-matrix of the HYP Smearing.

Blocking Steps	λ_1	λ_2	λ_3	λ_4	λ_5
1	3.9087	1.0241	0.5681	0.1646	0.0642
2	4.5181	2.5664	0.8697	0.8697	0.6949
3	2.0232	1.8503	0.9926	0.9926	0.8930
4	1.6052	1.4201	1.0331	1.0331	0.9464
5	1.3947	1.2413	1.0383	1.0383	0.9657
6	1.2238	1.1795	1.0515	1.0515	0.9715
7	1.1729	1.1619	1.0456	1.0456	0.9783
8	1.1862	1.1322	1.0339	1.0339	0.9844
9	1.1397	1.1068	1.0399	1.0399	0.9892
10	1.1257	1.0728	1.0728	1.0305	0.9939

Table 6.4: Eigenvalues of T-matrix of the n-HYP Smearing.

Blocking Steps	λ_1	λ_2	λ_3	λ_4	λ_5
1	2.5575	1.3786	1.0704	0.8438	0.3913
2	2.2061	1.3518	1.1657	0.9971	0.5390
3	1.8535	1.4271	1.0855	0.9688	0.7027
4	1.7100	1.4744	0.9537	0.9297	0.8941
5	1.5748	1.4088	0.9723	0.9723	0.9209
6	1.4578	1.3080	1.0209	0.9994	0.9297
7	1.3809	1.2373	1.0369	1.0105	0.9445
8	1.3223	1.1995	1.0263	1.0263	0.9579
9	1.2764	1.1732	1.0251	1.0251	0.9678
10	1.2385	1.1493	1.0231	1.0231	0.9754

Table 6.5: Eigenvalues of T-matrix of the STOUT Smearing.

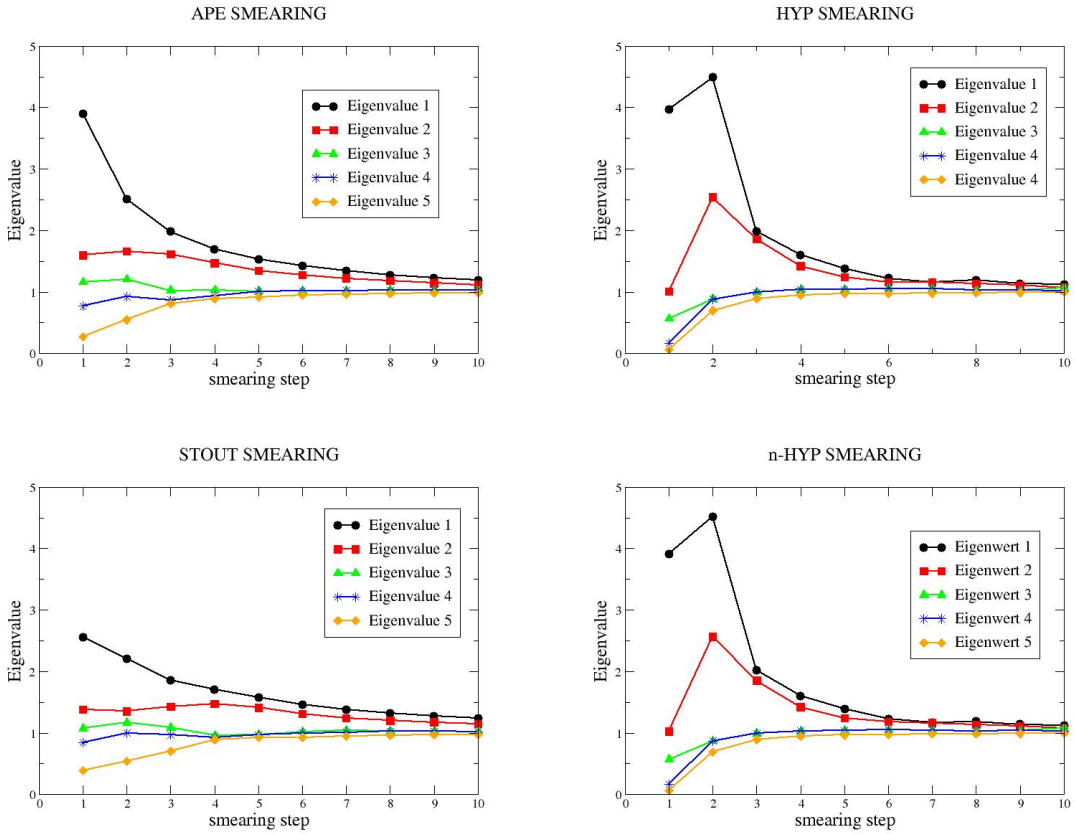

Figure 6.12: Flow behavior of the eigenvalues after repeated smearing steps.

These numbers are the eigenvalues of the T-matrix which gives the change of the n+1 times blocked coupling after another n times blocked coupling

$$T_{jk}^{(n+1,n)} = \frac{\partial \beta_j^{n+1}}{\partial \beta_k^n}.$$

The T-matrix gives the effect of the different kind of smearing methods. It characterizes the flow of the couplings. In the plots above we see how the eigenvalues change though the process of the repeated smearing procedures. The direction of the flow is equal for each of the smearing methods but the sharpness of the flow is quite different. For HYP and n-HYP smearing we get very similar flow picture. We have seen this kind of behavior also in the flow of the observables.

We can also plot our set of data for the eigenvalues in a another way to see the flow of the eigenvalues. Like in the case of the operators we plot eigenvalues on n times smeared configurations versus n+k times smeared configurations.

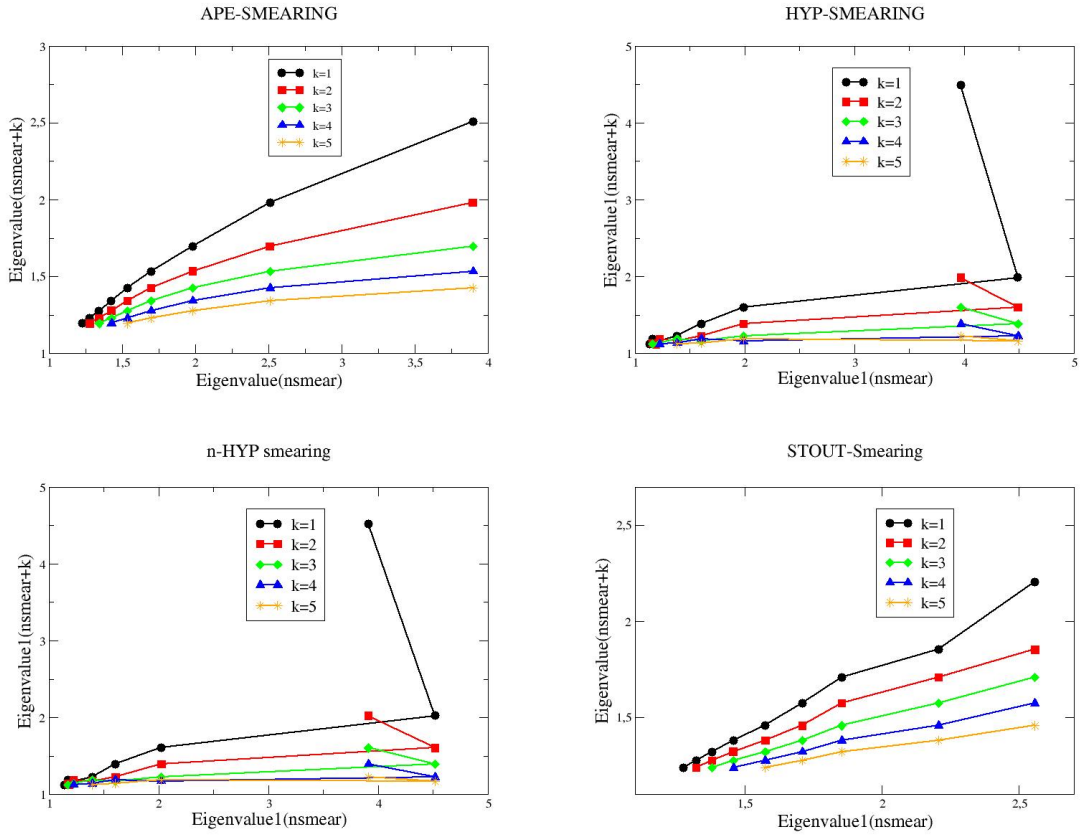

Figure 6.13: The first eigenvalue as a function of the smearing step versus the same eigenvalue as a function of smearing step plus k .

We see that the slopes of this lines is going to the zero if we increase our k. Using the fact that the decreasing of the slope corresponds to an more effective smearing, we can devise plots to compare the different smearing methods.

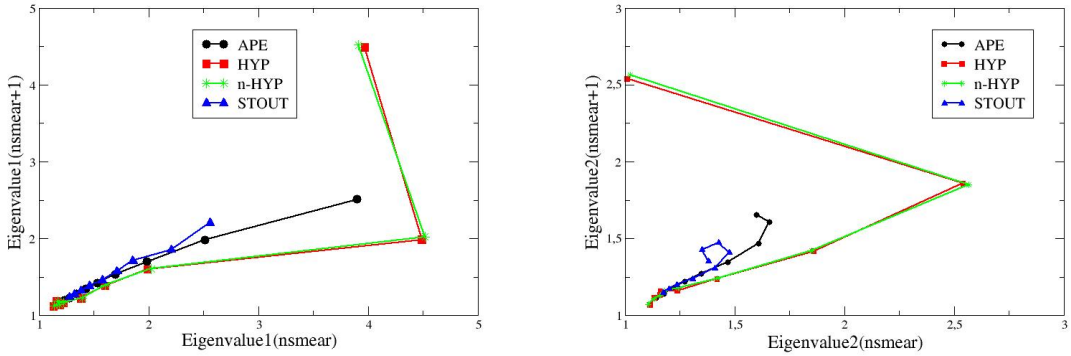

Figure 6.14: The first eigenvalue as a function of the smearing step versus the same eigenvalue as a function of smearing step plus 1 .

From these plots we see an affirmation of our previous results. HYP and n-HYP smearing are more effective that the other smearing procedures.

Monte Carlo renormalization group methods also supply the eigenvectors to these eigenvalues. Also the eigenvectors play an essential role since the components of an eigenvector gives the contribution of each operator to the flow. Therefore we study also the eigenvectors to these eigenvalues. As we have seen in the figures above the first eigenvalue is the dominant one. Therefore we study only the components of the first eigenvector and how much each operator contributes to the flow.

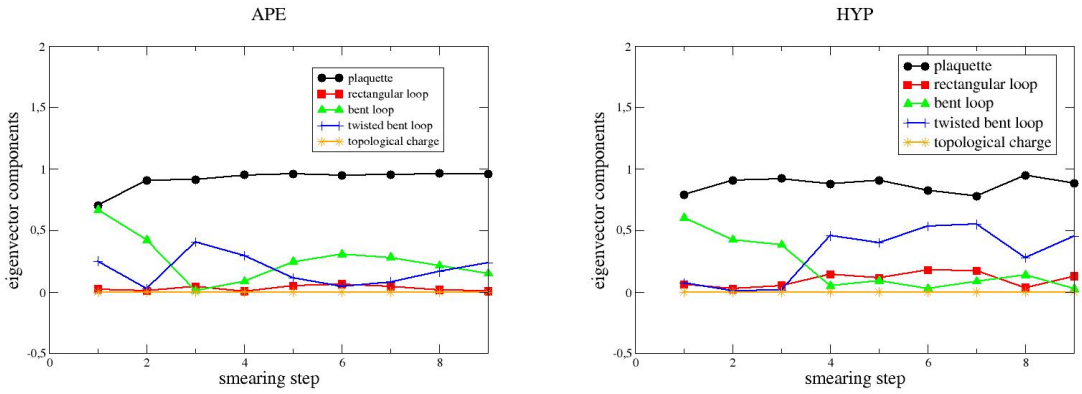

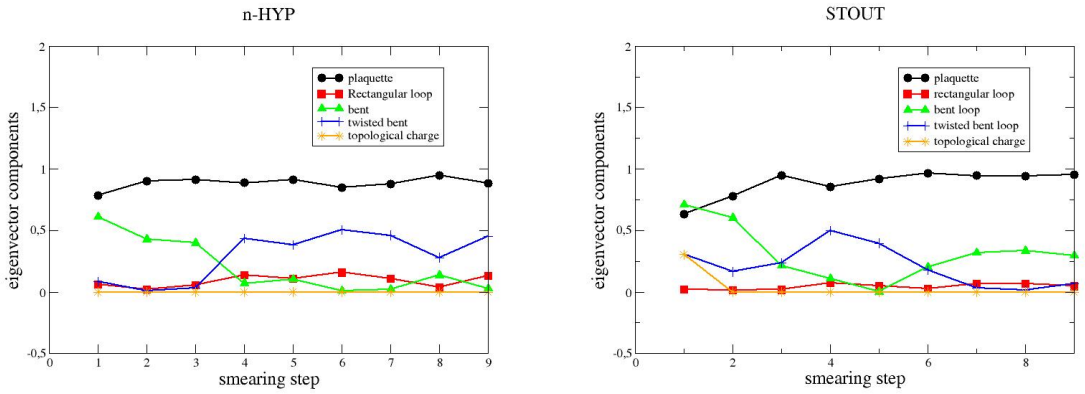

Figure 6.15: The behavior of the components of the first eigenvector which belongs to the first eigenvalue under repeated smearing steps.

Obviously we see that the dominant operator is the plaquette. Twisted bent and bent loop increase with the increasing levels of the smearing steps. The reason for this characteristics may be due the fact that increasing levels of smearing affect more and more neighbors of a link. In this way first smaller loops contribute more to the flow than the larger ones but within more smearing steps the contributions of larger loops increase. On the other side the contribution of the topological charge stays always near zero.

Like in the case for the flow behavior of observables we can also summarize some of our important facts which we gained from the analyze of the flow of the couplings.

(a) Various plots from the results of the T-matrix show the effect of the smearing methods. We view the different smearing methods as different block spin transformations. Our smearing methods shows similar flow behavior. The fixed point of the smearing methods is the same.

(b) The velocity of the smearing methods is different, also if one selects the smear parameter in such a way to maximize the flow. The flow speed of HYP and n-HYP smearing is almost equal. These two smearing procedures are in flow speed followed by APE smearing. STOUT smearing has the slowest speed.

(c) The leading contribution to the flow is given by the plaquette, the contributions of the twisted bent and bent increase with the increasing levels of the smearing.

7 Summary

Smearing procedures are an important ingredient in lattice QCD calculations, therefore it is worth to study them. We tried to analyze the efficiency of different smearing methods systematically, using the technique which was first time proposed by S. K. Ma referred to as Monte Carlo renormalization group, which is a combination of Monte Carlo methods and renormalization group.

We consider the smearing methods as scale transformations, so-called block spin transformations. Through this assumption we could apply standard tools of Real-Space Renormalization Group. We used some local observables corresponding to the couplings like in the case of spin systems with, e.g., next neighbor coupling, second neighbor etc. These observables are calculated on repeatedly smeared configurations. In this way the flow direction and the flowing speed of the smearing methods in operator space can be analyzed.

Then we use cross-correlations to switch from the operator space to the coupling space. There we linearize our coupling flow and find a T-matrix, whose eigenvalues characterize and quantify the flow of the couplings under smearing transformations.

All of these calculations provide important information about the effectiveness of a smearing method. The comparison of different smearing methods in this analysis helps us to estimate some kind of ratio between these smearing methods. This ratio gives us the information about how many smearing steps in one smearing method corresponds to how many smearing steps in another smearing method. In this way one can combine some of the smearing methods to achieve a desired effectiveness, which is of interest.

Our analysis gives some kind of footprint for each smearing method. So this could help to construct more effective smearing methods.

Finally we comment about on our analysis of the smearing methods. The experience of some physicist working in this area about the effectiveness of the smearing methods can be reconstructed without having any knowledge about the effectiveness of the smearing methods with our analysis. We could really reach a systematically analysis of the smearing methods which we treated. Our analysis delivers good information about smearing methods and about their comparison.

Bibliography

[1] K. G. Wilson, "Confinement and Quarks," *Phys. Rev. D* **10** (1974) 2445.

[2] D. Griffths, *Introduction to Elementary Particles*. John Wiley Sons,inc., New York, 1987.

[3] M. E. Peskin and D. V. Schoeder, *An Introduction to Quantum Field Theory*. Westview Press, Colorado, 1995.

[4] H. Weyl, "Electron und Gravitation," *Zeit. f. Physik* **56** (1929) 330.

[5] C. N. Yang and R. L. Mills, "Conservation of Isotopic Spin and Isotopic Gauge Invariance," *Phys. Rev.* **96** (Oct, 1954) 191–195.

[6] O. W. Greenberg, "Spin and Unitary-Spin Independence in a Paraquark Model of Baryons and Mesons," *Phys. Rev. Lett.* **13** (Nov, 1964) 598–602.

[7] H. L. H. Fritzsch, M. Gell-Mann, "Advantages of the Color Octet Gluon Picture," *Phys. Lett. B* **47** (1972) 365.

[8] R. MacKenzie, "Path Integral Methods and Applications," `arXiv:quant-ph/0004090`.

[9] C. Gattinger and C. B. Lang, *Quantum Chromodynamics on the Lattice*. Springer Verlag, München, 2009.

[10] M. Creutz, "Lattice Gauge Theories and Monte Carlo Algorithms," *Nucl. Phys. B (Proc. Suppl.)* **10 A** (1989) 1–22.

[11] N. Metropolis, A. W. Rosenbluth, M. N. Rosenbluth, A. H. Teller, and E. Teller, "Equations of state calculations by fast computing machines," *J. Chem. Phys.* **21** (1953) 1087.

[12] W. Hastings, "Monte Carlo Sampling Methods Using Markov Chains and Their Applications," *Biometrika* **57** (1970) 97–109.

[13] M. Creutz, "Monte Carlo Study of Quantized SU(2) Gauge Theory," *Phys. Rev. D* **21** (1980) 2308.

[14] S. Duane, A. D. Kennedy, B. J. Pendleton, and D. Roweth, "Hybrid Monte Carlo," *Phys. Lett.* **B195** (1987) 216–222.

[15] F. Fucito, E. Marinari, G. Parisi, and C. Rebbi, "A Proposal for Monte Carlo Simulations of Fermionic Systems," *Nucl. Phys. B* **180** (1981) 369.

[16] D. H. Weingarten and D. N. Petcher, "Monte Carlo Integration for Lattice Gauge Theories with Fermions," *Phys. Lett. B* **99** (1981) 333.

[17] W. Kamleh, D. B. Leinweber, and A. G. Williams, "Hybrid Monte Carlo Algorithm with Fat Link Fermion Actions," *Phys. Rev. D* **70** (Jul, 2004) 014502.

[18] D. J. E. Callaway and A. Rahman, "Lattice Gauge Theory in the Microcanonical Ensemble," *Phys. Rev. D* **28** (1983) 1506.

[19] M. C. Chu, J. M. Grandy, S. Huang, and J. W. Negele, "Evidence for the Role of Instantons in Hadron Structure from Lattice QCD," *Phys. Rev. D* **49** (1994) 6039–6050.

[20] **APE** Collaboration, M. Albanese *et al.*, "Glueball Masses and String Tension in Lattice QCD," *Phys. Lett. B* **192** (1987) 163.

[21] F. D. R. Bonnet, D. B. Leinweber, A. G. Williams, and J. M. Zanotti, "Improved Smoothing Algorithms for Lattice Gauge Theory," *Phys. Rev.* **D65** (2002) 114510, `arXiv:hep-lat/0106023`.

[22] C. Morningstar and M. Peardon, "Analytic Smearing of SU(3) Link Variables in Lattice QCD," *Phys. Rev. D* **69** (2004) 054501, `arXiv:hep-lat/0311018`.

[23] T. T. Takahashi, H. Matsufuru, Y. Nemoto, and H. Suganuma, "Three-Quark Potential in SU(3) Lattice QCD," *Phys. Rev. Lett.* **86** (Jan, 2001) 18–21.

[24] K. D. Asit, A. Harindranath, and M. Jyotirmoy, "Investigation of Lattice QCD with Wilson Fermions with Gaussian Smearing," `arXiv:hep-lat/0712.4354`.

[25] S. Capitani, S. Durr, and C. Hoelbling, "Rationale for UV-Filtered Clover Fermions," *JHEP* **11** (2006) 028, `arXiv:hep-lat/0607006`.

[26] A. Hasenfratz, R. Hoffmann, and F. Knechtli, "The Static Potential with Hypercubic Blocking," *Nucl. Phys. B (Proc. Suppl.)* **106** (2002) 418, `arXiv:hep-lat/0110168`.

[27] C. Gattringer, E. M. Ilgenfritz, and S. Solbrig, "Cooling, Smearing and Dirac Eigenmodes: A Comparison of Filtering Methods in Lattice Gauge Theory," `arXiv:hep-lat/0601015`.

[28] K. J. Juge, A. Lichtl, C. Morningstar, R. G. Edwards, D. G. Richards, S. Basak, S. Wallace, I. Sato, and G. T. Fleming, "Towards a Determination of the Spectrum of QCD Using a Space-Time Lattice," `arXiv:hep-lat/0601029`.

[29] A. Hasenfratz, R. Hoffmann, and S. Schaefer, "Hypercubic Smeared Links for Dynamical Fermions," *JHEP* **05** (2007) 029, `arXiv:hep-lat/0702028`.

[30] S. Schaefer, A. Hasenfratz, and R. Hoffmann, "Dynamical Simulations with HYP-Link Wilson Fermions," *PoS* **LAT2007** (2007) 132, arXiv:hep-lat/0709.4130.

[31] S. Durr, "Logarithmic Link Smearing for Full QCD," *Comput. Phys. Commun.* **180** (2009) 1338–1357, arXiv:hep-lat/0709.4110.

[32] N. Cabibbo and E. Marinari *Phys. Lett. B* **119** (1982) 387.

[33] J. Hoek, "Optimized Monte Carlo Renormalization Group Transformations for SU(3) Lattice Gauge Theory," *Nucl. Phys. B* **329** (1990) 240.

[34] F. D. R. Bonnet, P. Fitzhenry, D. B. Leinweber, M. R. Stanford, and A. G. Williams, "Calibration of Smearing and Cooling Algorithms in SU(3)- Color Gauge Theory," *Phys. Rev.* **D62** (2000) 094509, arXiv:hep-lat/0001018.

[35] Y. Liang, K.-F. Liu, B.-A. Li, S. J. Dong, and K. Ishikawa, "Lattice Calculation of Glueball Matrix Elements," *Phys. Lett.* **B307** (1993) 375–382, arXiv:hep-lat/9304011.

[36] C. W. Bernard and T. A. DeGrand, "Perturbation Theory for Fat-Link Fermion Actions," *Nucl. Phys. Proc. Suppl.* **83** (2000) 845–847, arXiv:hep-lat/9909083.

[37] S. Durr, "Gauge Action Improvement and Smearing," *DESY 04-177, SFB/CPP-04-49* **180** (2005) 1338–1357, arXiv:hep-lat/0409141v2.

[38] C. Gattringer, R. Hoffmann, and S. Schaefer, "Setting the Scale for the Lüscher-Weisz Action," *Phys. Rev. D* **65** (Apr, 2002) 094503.

[39] C. B. Lang, P. Majumdar, and W. Ortner, "First Results from Dynamical Chirally Improved Fermions," *PoS* **LAT2005** (2005) 131, arXiv:hep-lat/0509005.

[40] C. Gattringer, C. Hagen, C. B. Lang, M. Limmer, D. Mohler, and A. Schäfer, "Hadron Spectroscopy with Dynamical Chirally Improved Fermions," *Phys. Rev. D* **79** (2009) 054501, arXiv:hep-lat/0812.1681.

[41] P. W. Martin Lüscher, "On-shell Improved Lattice Gauge Theories," *Commun. Math. Phys.* **97** (1985) 59–77.

[42] M. Luscher, "Topology of Lattice Gauge Fields," *Commun. Math. Phys.* **85** (1982) 39.

[43] F. Bruckmann, C. Gattringer, E.-M. Ilgenfritz, M. Müller-Preussker, A. Schafer, and S. Solbrig, "Quantitative Comparison of Filtering Methods in Lattice QCD," *Eur. Phys. J.* **A33** (2007) 333–338, arXiv:hep-lat/0612024.

[44] F. Bruckmann, F. Gruber, C. B. Lang, M. Limmer, T. Maurer, A. Schäfer, and S. Solbrig, "Comparison of Filtering Methods in SU(3) Lattice Gauge Theory," *PoS* **CONFINEMENT8** (2008) 045, arXiv:hep-lat/0901.2286.

[45] C. Gattringer, I. Hip, and C. B. Lang, "Approximate Ginsparg-Wilson fermions: A first test," *Nucl. Phys. B* **597** (2001) 451, `arXiv:hep-lat/0007042`.

[46] C. Gattringer, "A New Approach to Ginsparg-Wilson Fermions," *Phys. Rev. D* **63** (2001) 114501, `arXiv:hep-lat/0003005`.

[47] S.-k. Ma, "Renormalization Group by Monte Carlo Methods," *Phys. Rev. Lett.* **37** (1976) 461–464.

[48] T. W. Burkhardt and J. M. J. van Leeuwen, "Progress and Problems in Real-Space Renormalization," in *Real-space Renormalization*, T. W. Burkhardt and J. M. J. van Leeuwen, eds., p. 1. Springer-Verlag, Heidelberg, 1982.

[49] R. Baier, C. B. Lang, and H.-J. Reusch, "The Renormalization Flow in the Adjoint $SU(2)$ Lattice Higgs Model," *Nucl. Phys. B* **305 [FS23]** (1988) 396.

[50] R. H. Swendsen, "Monte Carlo renormalization group," *Phys. Rev. Lett.* **42** (1979) 859.

[51] R. H. Swendsen, "Monte Carlo Renormalization-Group Studies of the $d = 2$ Ising Model," *Phys. Rev. B* **20** (Sep, 1979) 2080–2087.

[52] R. H. Swendsen, "Monte Carlo Renormalization-Group Study of the $d = 3$ Planar Model," *Phys. Rev. B* **27** (Jan, 1983) 391–400.

[53] A. Patel, "Monte Carlo Renormalisation Group for QCD," Ph.D Thesis, California Institute of Technology, 1984.

[54] C. B. Lang, "Computer Stochastics in Scalar Quantum Field Theory," in *Stochastic Analysis and Applications in Physics: Proc. of the NATO ASI in Funchal, Madeira, Aug. 1993*, A. I. Cardoso, M. de Faria, J. Potthoff, R. S´en´eor, and L. Streit, eds., pp. 133–192. NATO ASI Series C - Vol. 449 (Kluwer Academic Publishers), Dordrecht, 1994.

Acknowledgements

Ich möchte mich als erstes bei meinem Betreuer Prof. Christian B. Lang zur Verfügung dieses Themas für die sehr kompotente Betreuung und für die Geduld bedanken.

Desweiteren beim Prof. Christoph Gattringer für die Unterstützung während der Diplomarbeit bedanken. Ich möchte mich auch bei den anderen Mitgliedern der Lattice Quantum Field Theory Research Group und bei meinen Studien Kollegen bedanken.

Bu vesileyle ailemede tesekkür etmek isterim. Ögrenme hayatimda bana yaptiklari amansiz bitmek tükenmez katkilarindan dolayi.